CDF/DOC/TRACKING/CDFR/5080
October 25, 1999
Version 1.0

Charge Deposition Model in Silicon

P. Azzi, N. Bacchetta, G. Martignon, M. Menguzzato, A. Ribon, R. Rossin

Padova University and INFN, Padova

Abstract

We present here a charge deposition model in Silicon that, relying only on first principles, can be used as a tool for general description of silicon microstrip detectors with single and double sided readout. This model describes well both SVX' Run 1 data and test beam data with SVXII sensors. Once integrated in the full CDFII simulation package, this model will allow to predict and follow the performances of the Silicon system in Run2 as a function of time and integrated luminosity.

1 Introduction

The main motivation for this model are obvious since in the current simulation there was no model of charge deposition in Silicon[2] apart from a purely geometrical one. All the studies needed to evaluate the performances of the tracking in the Silicon system rely on a reasonable cluster shape. Moreover, in the past CDF always lacked a good description of the charge deposition obtained only from first principles, and a big improvement in the hit simulation was obtained with the SVX' MC through the use of a parametrization of the data themselves. However, since in the incoming run the running conditions, the radiation damage and so the performances will be different for different parts of the Silicon tracking system we have developed a tool that could be tuned to the various pieces of the detector, able to predict the variation in their performances and that can be used easily for studies of new detector configuration (i.e. L00). The idea is to have the capability of monitoring, predicting and comparing the electrical behaviour of the real detector with the expectation from the theory.

In Chapter 2 the details of the primary charge deposition mechanism, δ-rays generations, diffusion modeling, magnetic field and noise effects are described. In Chapter 3 are shown the results of the comparison of this simulation with real data from the 1997 Test Beam (SVXII type sensors) and Run 1 (SVX'). In Chapter 4 this simulation program is used to evaluate the performances in term of single hit resolution and two hits separation of different sensor configuration for the L00 project. Conclusions are in Chapter 5.

2 Details of the model

2.1 Primary charge

An incident track is stepped through the Silicon (with an assumed thickness of $L = 300\,\mu$m) in $10\,\mu$m steps progressing at the angle of incidence. At each step the energy deposited is calculated using a Landau distribution of average given by the restricted energy loss formula [1]:

$$\left.\frac{-dE}{dx}\right|_{T<T_{cut}} = Kz^2\frac{Z}{A}\frac{1}{\beta^2}\left[\frac{1}{2}\ln\frac{2m_ec^2\beta^2\gamma^2T_{upper}}{I^2} - \frac{\beta^2}{2}\left(1+\frac{T_{upper}}{T_{max}}\right) - \frac{C}{Z} - \frac{\delta}{2}\right]$$

where T_{max} is the maximum kinetic energy which can be imparted to a free electron in a single collision. Since we are dealing with a small tracking volume and energetic δ-rays above 500 KeV escape from the sensor, as described in the next paragraph, we set the arbitrary parameter $T_{cut} = 500\,$KeV. Finally, $T_{upper} = MIN(T_{cut}, T_{max})$, whereas the other variables are defined in [1].

[2]This is not true anymore see CDF Note 4914 and 5069

The second parameter that defines a Landau distribution is the Landau width defined as:

$$W = L_{\text{effective}} \frac{2\pi e^4}{m_e c^2} \frac{1}{\beta^2} \rho N_A \frac{Z}{A} \tag{1}$$

where $L_{\text{effective}}$ is the real path length travelled by the ionizing particle (for normal incidence $L_{\text{effective}} = L = 300\,\mu$m, i.e. typical Silicon thickness). The Landau distribution must be convoluted with a Gaussian to take in account the fact that the electrons are bounded and not completely free [2]: the σ of the Gaussian is about 6 KeV in 300 μm of Silicon, see Fig.1.

An electron-hole pair is created at the center of the sub-cell for every 3.6 eV of energy deposited and is then diffused toward the electrodes.

A factor two in speed of this simulation can be obtained increasing the steps from 10 μm to 30 μm with a negligible effect on the significant distributions (cluster charge, cluster size and residuals). See Fig.2 and Fig.3 for a comparison.

2.2 Delta rays

The energy interval considered for the generation of δ-rays goes from 10 KeV up to 500 KeV. The range for a δ-ray of 10 KeV is about 1 μm and becomes $\geq 600\,\mu$m for energies $T \geq 500$ KeV. The probability to generate a δ-ray of energy $T \geq 10$ KeV is about 50%, while for $T \geq 500$ KeV is about 1% . The differential distribution used for δ-rays between [T,T+δT] (for spin 0 particles, i.e. a good approximation since π and K are the most probable incident particles) is given by [3]:

$$(\frac{dN}{dT}) \cdot dT = (\frac{W}{T^2}) \times (1 - \beta^2 \times \frac{T}{T_{max}}) \cdot dT$$

where W is Landau width defined in (1). The range is obtained from the semiempirical formula in [4] while the energy released by the δ-ray along its trajectory in the interval between $(x, x + dx)$ comes from the relation:

$$\left(\frac{dE}{dx}\right) \cdot dx = \frac{T}{2 \cdot R\sqrt{(1 - \frac{x}{R})}} \cdot dx$$

where T is the kinetic energy of the δ-ray, R its effective 3D range and x its 3D distance from the origin. Finally, the θ polar angle of the δ-ray direction with respect to the incident track is obtained through energy conservation, while the ϕ angle is drawn randomly from a flat distribution between [0,2π]. Few approximations have been made in the δ-ray modeling:

- δ rays trajectories are straight lines

[3] This is obtained from [3] after integration in x.

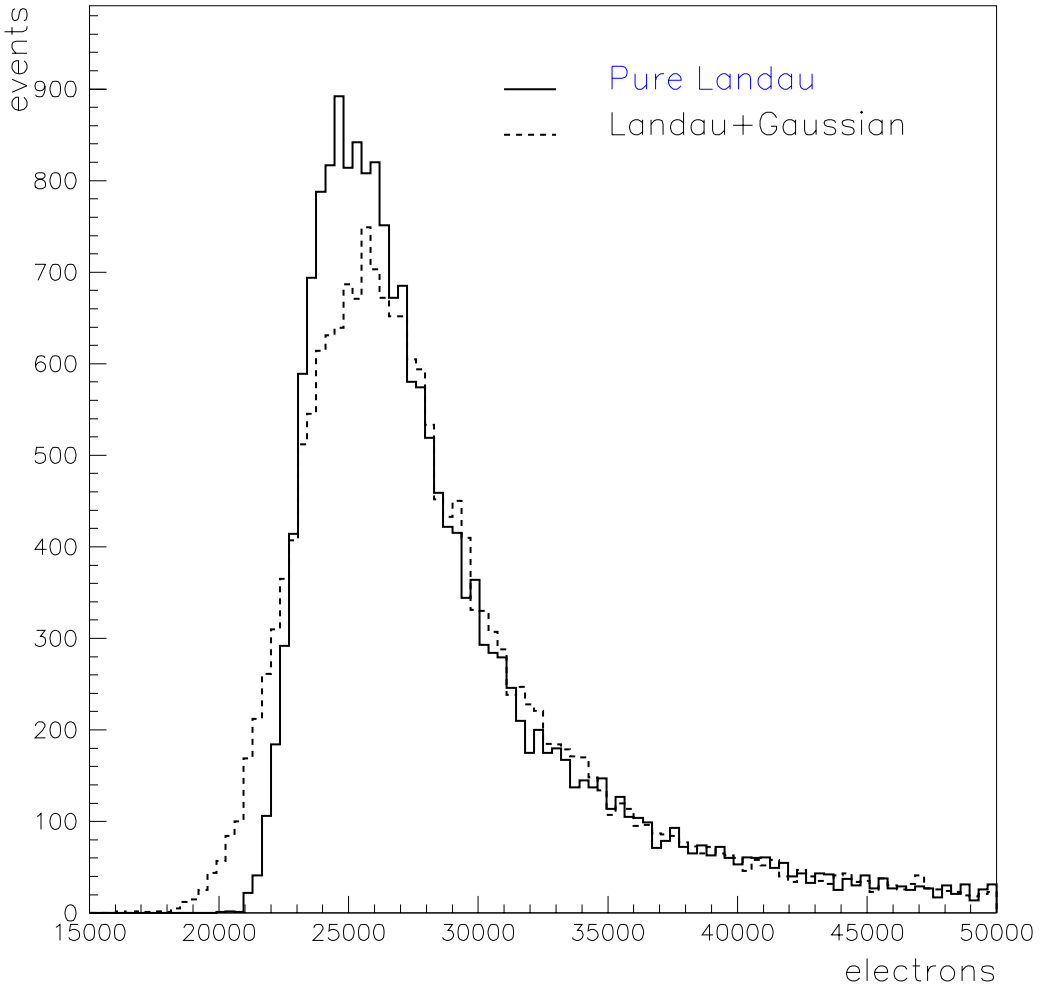

Figure 1: Comparison of the pure Landau distribution obtained from the Bethe-Bloch with the Landau convoluted with a Gaussian to take in account the fact that the electrons in the Silicon are not free. This is a more correct physical description, however the effect is very small.

- no effect of the B field on the trajectory (but effect of the magnetic field considered on the diffused charge)
- δ rays do not originate other secondary δ-rays
- no loopers, that is δ rays that escape the Silicon with sufficient energy that the B field would make them spiral back into the Silicon. This effect however is treated correctly in the full simulation because Geant takes the list of the

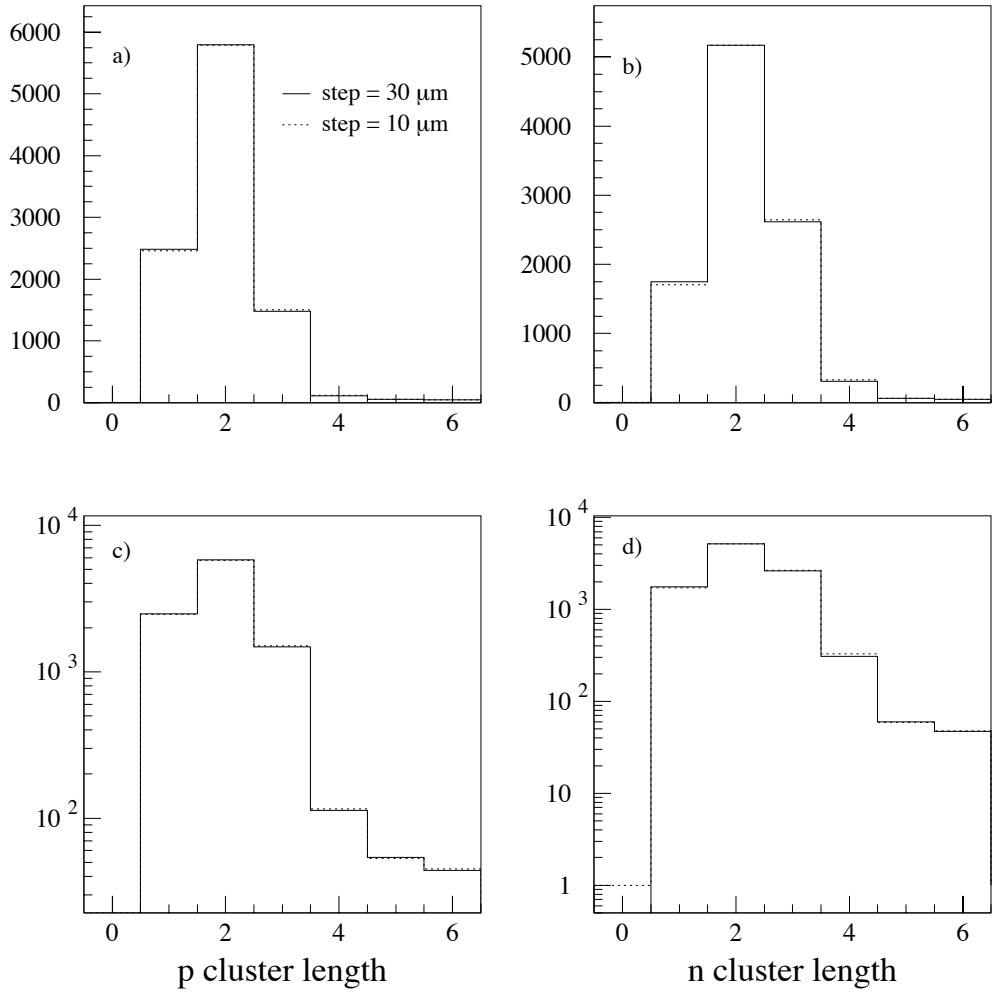

Figure 2: Comparison of the cluster size for two different choices of the steps for primary charge deposition through the Silicon. Tracks incident at angles $15^o \leq \phi \leq 165^o$ and $70^o \leq \theta \leq 110^o$. *a*),*b*) linear scale; *c*),*d*) log scale.

escaping particles.

2.3 Magnetic field effect

The presence of the magnetic field affects the mean position ("Lorentz angle" shift called $\Delta_{Lorentz}$) and the shape of the diffused charge:

$$\Delta_{Lorentz}(e,h) = d \times \tan\theta_H = d \times \mu(e,h) \times B_{field}$$

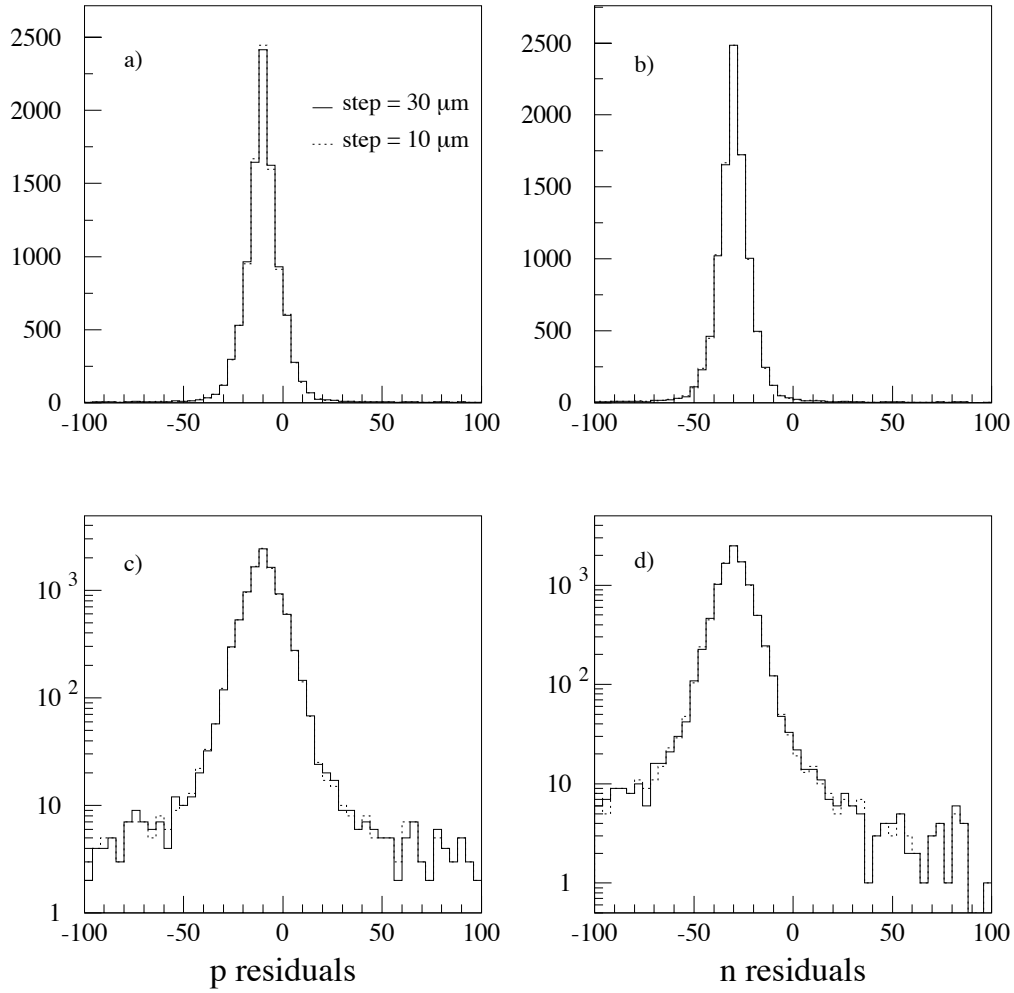

Figure 3: Comparison of the residual distribution for two different choices of the steps for primary charge deposition through the Silicon. Tracks incident at angles $15^o \leq \phi \leq 165^o$ and $70^o \leq \theta \leq 110^o$. *a*),*b*) linear scale; *c*) and *d*) log scale

where d is the distance of the charge carrier from the respective cathod. The mobility μ is given by:

$$\mu = \mu_{min} + \frac{\mu_0}{(1 + (\frac{N}{N_{ref}})^{\alpha})}$$

where N is the doping and all other quantities are fit parameters that depend on the temperature as $A = A_0(T/300^o)^n$. Since the impurity level of our Silicon is very

small ($N < 10^{14}\,\mathrm{cm}^{-3}$) we can safely approximate the formula to

$$\mu = \mu_{min}(T) + \mu_0(T)$$

but we take into account the dependence on the temperature.

parameters	*electrons*	*holes*	n
$\mu_{min}\,(\mathrm{cm}^2/\mathrm{Vs})$	92	54.3	-0.57
$\mu_0\,(\mathrm{cm}^2/\mathrm{Vs})$	1268	406.9	-2.33 (e)/-2.23 (h)
$N_{ref}\,(\mathrm{cm}^{-3})$	$1.30 \cdot 10^{17}$	$2.35 \cdot 10^{17}$	2.4

The mobility($cm^2/V \cdot s$) is approximately $\mu(e) = 1540$ and $\mu(h) = 519$ at $T = 10^o$ C. In a 1.4 T magnetic field this corresponds in a shift of the drifting trajectory of $tan\theta_H = \mu \times B$ that corresponds for 150 μm in silicon to about $\Delta_H(electrons) = 31.5\,\mu m$, $\Delta_H(holes) = 10.9\,\mu m$. In Fig.4 and Fig.5 are shown the shifts to the residuals' mean and the change in the cluster size due to the presence of the magnetic field for holes and electrons in the case of normal incidence tracks. Note that the shift is in the same direction for electron and holes (electron have opposite charge and travel in an opposite direction wrt the holes).

2.4 Diffusion modeling

We assume a gaussian model for the diffusion width:

$$\sigma = \sqrt{2Dt}$$

where

$$D = \frac{kT}{q} \times \mu$$

and $t = distance/(\mu E)$. Once the electric field is expressed in terms of $V_{depletion}$, V_{bias}, wafer thickness and position inside the Silicon (w.r.t. n-side) the expressions of the diffusion σ becomes (before inversion):

$$\sigma^2_{holes}(x) = \frac{kT \cdot L^2}{e \cdot V_d} \times ln(\frac{V_{bias} - V_d + 2 \cdot V_d}{V_{bias} - V_d + x \cdot 2 \cdot \frac{V_d}{L}})$$

$$\sigma^2_{elec}(x) = \frac{kT \cdot L^2}{e \cdot V_d} \times ln(\frac{V_{bias} - V_d + x \cdot 2 \cdot \frac{V_d}{L}}{V_{bias} - V_d})$$

For the same V_d and V_{bias} after inversion the relations are still valid provided the exchange of $x \rightarrow (L - x)$ and $holes \rightarrow electrons$. This symmetry relies on the fact that the σ does not depend on the mobility of the drifting charges but only on the gradient of the electric field across the sensor, see Fig.6.

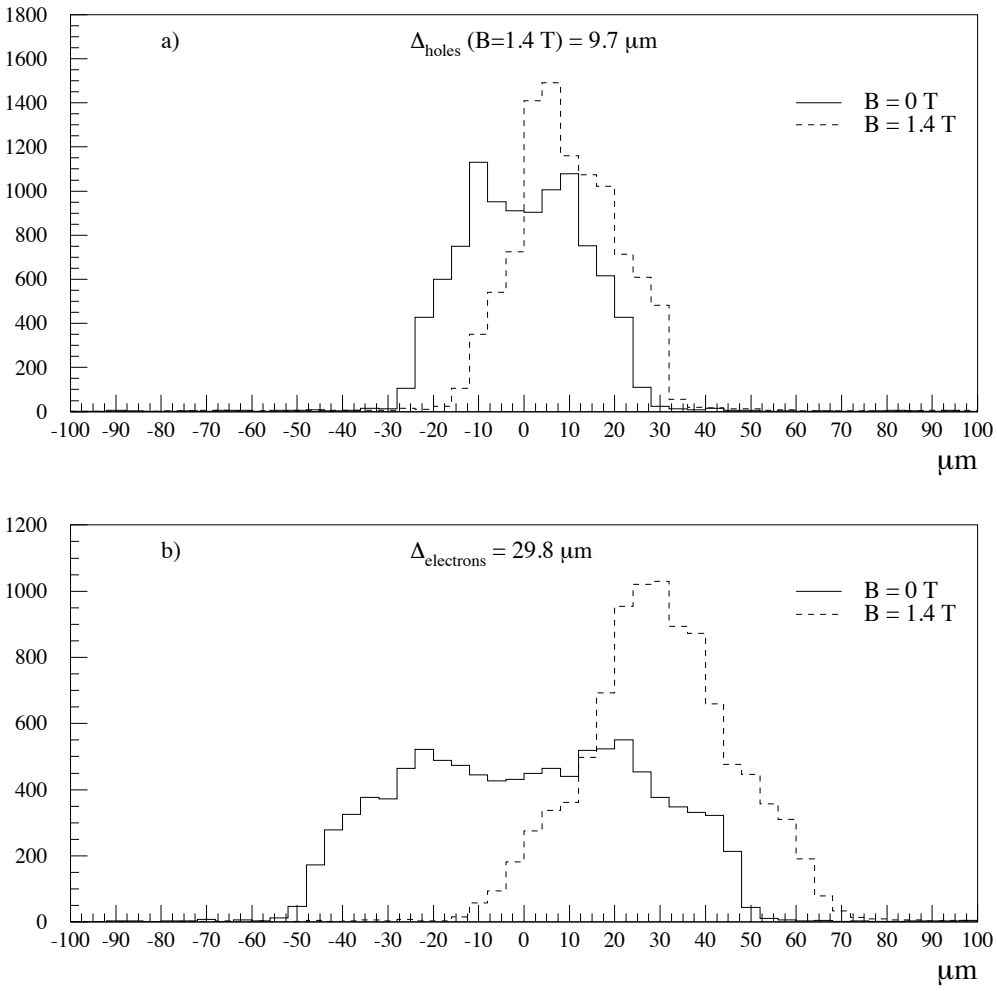

Figure 4: Distribution of the residuals for holes (a) and electrons (b) with and without magnetic field for normal incidence tracks. The noise is $1000\,e$. The shift is $\Delta \approx 10\,\mu m$ for the holes and $\Delta \approx 30\,\mu m$ for the electrons, as expected.

The average σ for a $300\,\mu$m path length is about $10\,\mu$m. In Fig.7 are shown the diffusion widths as a function of distance from the electrodes for different V_{bias} configurations.

The magnetic field also modifies the diffusion σ increasing it by a factor $1/cos\theta_H$. Moreover the intersection of the 2D gaussian with the sensor boundary becomes an ellipse where the major axis, seen by the $r-\phi$ strips is a factor $1/cos\theta_H$ bigger that the minor axis.

The diffusion width depends on V_{bias} and the temperature and this will have an effect

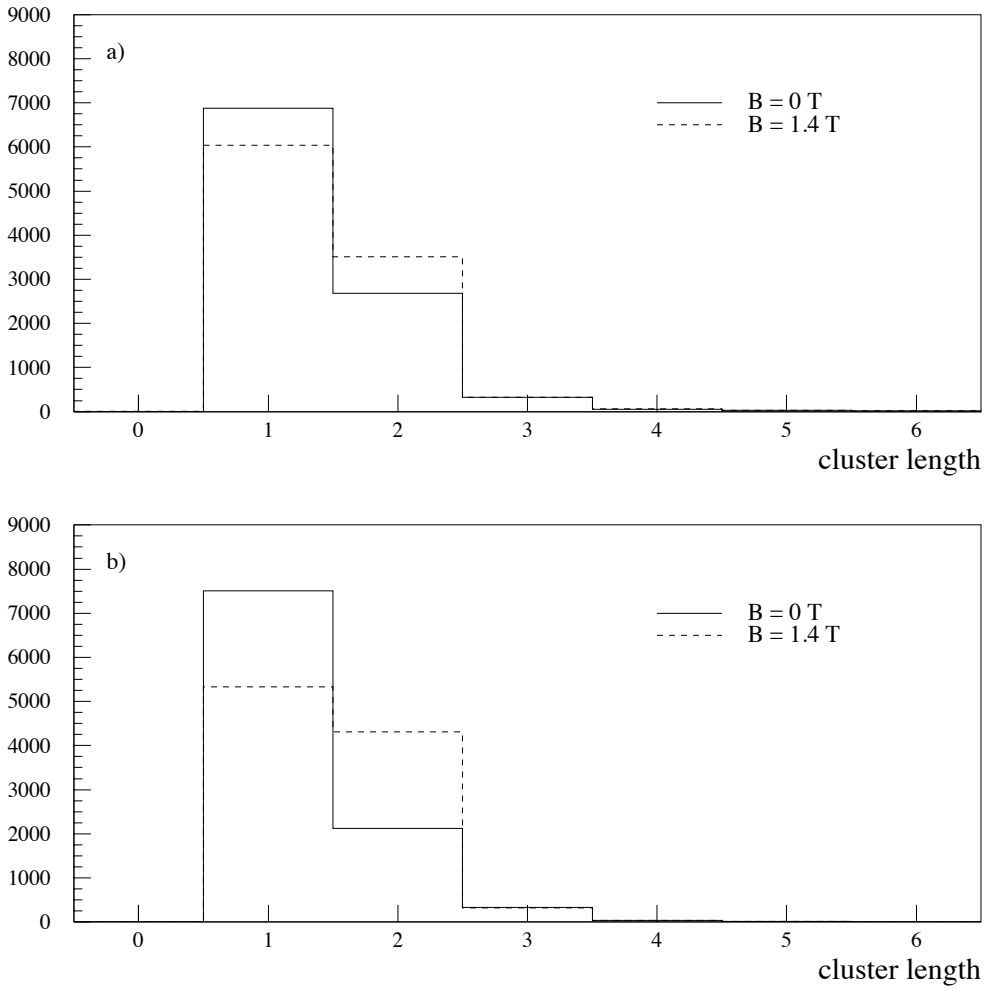

Figure 5: Distribution of the cluster size for holes (a) and electrons (b) with and without magnetic field for normal incidence tracks. The noise is 1000 e. The average cluster size wides due to the presence of the magnetic field and in particular the effect is bigger for the electrons that have a higher mobility.

on the cluster size. The variation of the average cluster size[4] as a function of the applied V_{bias} is shown in Fig.8, and as a function of the temperature in Fig.9.

[4]Since these effects are small compared to others, in order to appreciate them the noise and δ-rays have been turned off. Consequently only the behaviour of the cluster size is meaningful but not its value.

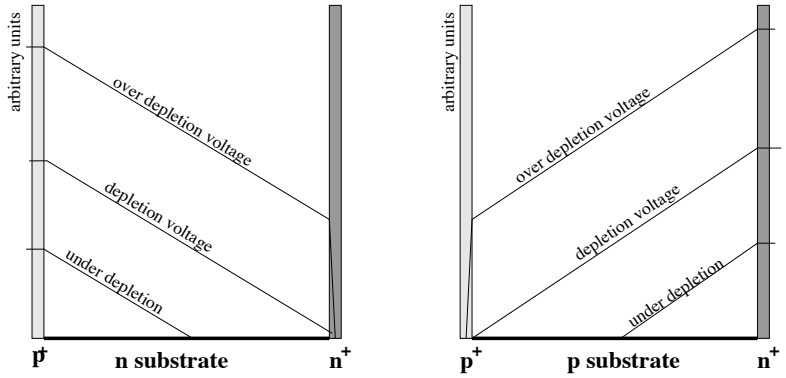

Figure 6: Electric field intensity as a function of the substrate thickness before and after type inversion. From this simple drawing is easier to picture the simmetry of the electric field behaviour.

2.5 Recombination

A fraction of the charge released in the primary ionization can recombine before reaching the electrode. In this simulation, this fraction is assumed to be a linear function of the distance from the production point of the charge to the readout end[5].

2.6 Noise and other readout effects

The noise in electrons is added to the generated signal for each strip using a gaussian distribution of mean 0 and σ given by the noise value. At the moment a fixed value is used that can be set through user input.

A fraction of the total charge can be lost due to several effects: capacitive coupling to the readout electronics, finite integration time, and recombination of the charge carriers before reaching the implants. The net effect is to shift toward lower values the position of the Landau peak. All these effects are summarized in a single parameter called "lost charge" that can be set via the user input.

The cross talk factor depends upon the ratio between the interstrip capacitance and the coupling capacitance. Nonetheless, experimental data shows that there is not a simple relation that can be applied for all cases and the typical value of this factor lies between 4% and 10%. Also this parameter can be set as input value.

2.7 p-n charge correlation

In Fig.10 is shown the charge correlation between the p and n-side. All the effects are included. Clustering requires a seed strip with a charge greater than 5σ and then looks for a set of adjacent strips over 4σ. δ-rays, noise and all other effects are included.

[5]This feature is present but not used at the moment.

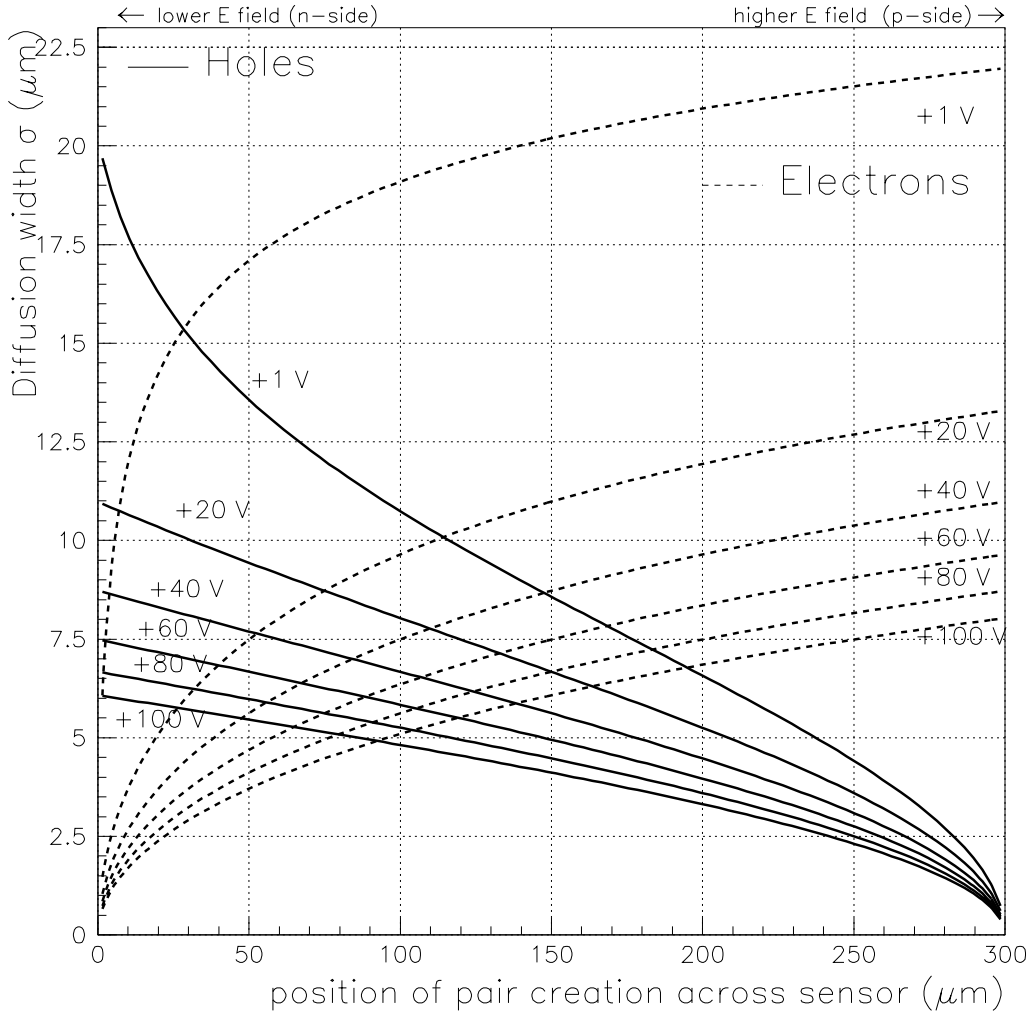

Figure 7: Curves of the diffusion σ (μm) for electrons and holes as a function of the traversed detector thickness. The curves are plotted for different values of the $\Delta V = V_{bias} - V_d$ with $V_d = 20\,\mathrm{V}$. The coordinate x=0 (300) μm corresponds to the n-side(p-side). These curves are valid before inversion: after inversion is sufficient to exchange $x \rightarrow (300 - x)$ and $holes \rightarrow electrons$.

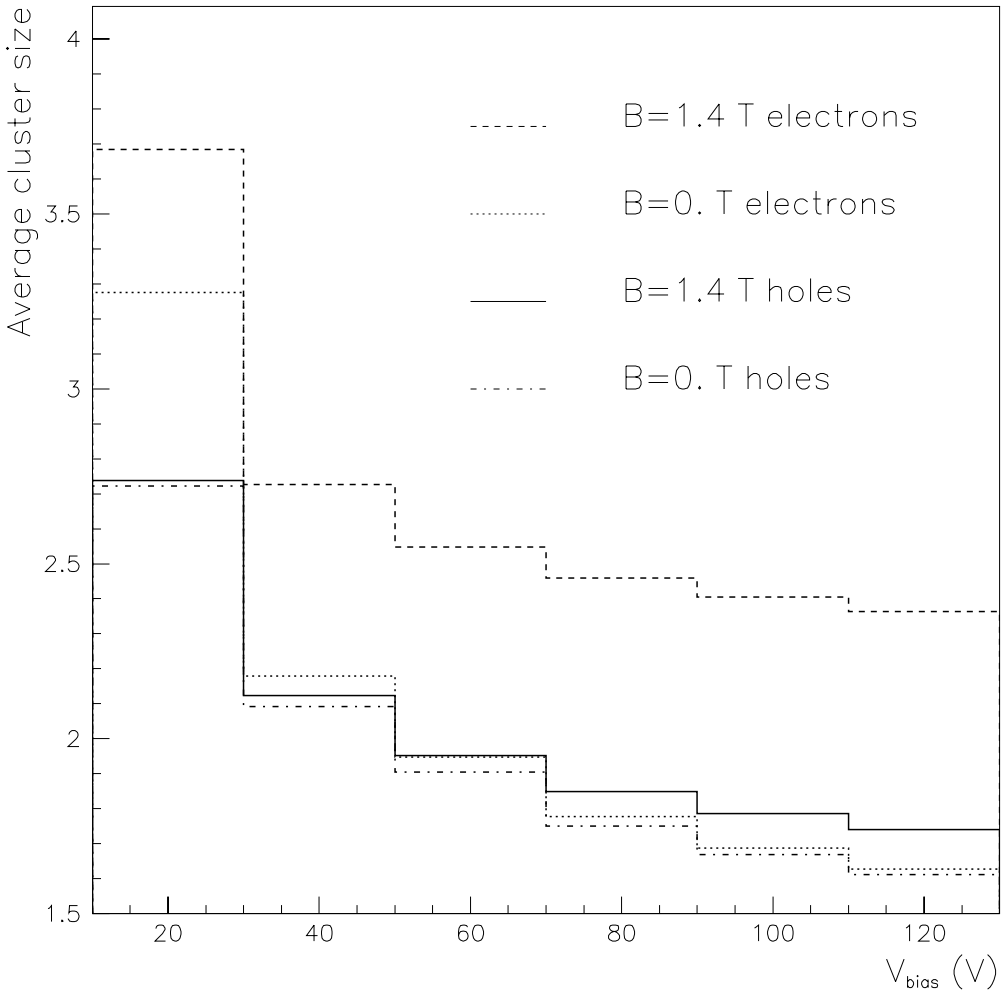

Figure 8: Average cluster size for normal incidence tracks as a function of V_{bias} for a 60 μm sensor with small angle stereo strips on the n-side. As expected the average cluster size gets smaller increasing the electric field (i.e. V_{bias}). To enhance the effect the noise and the δ-rays have been turned off.

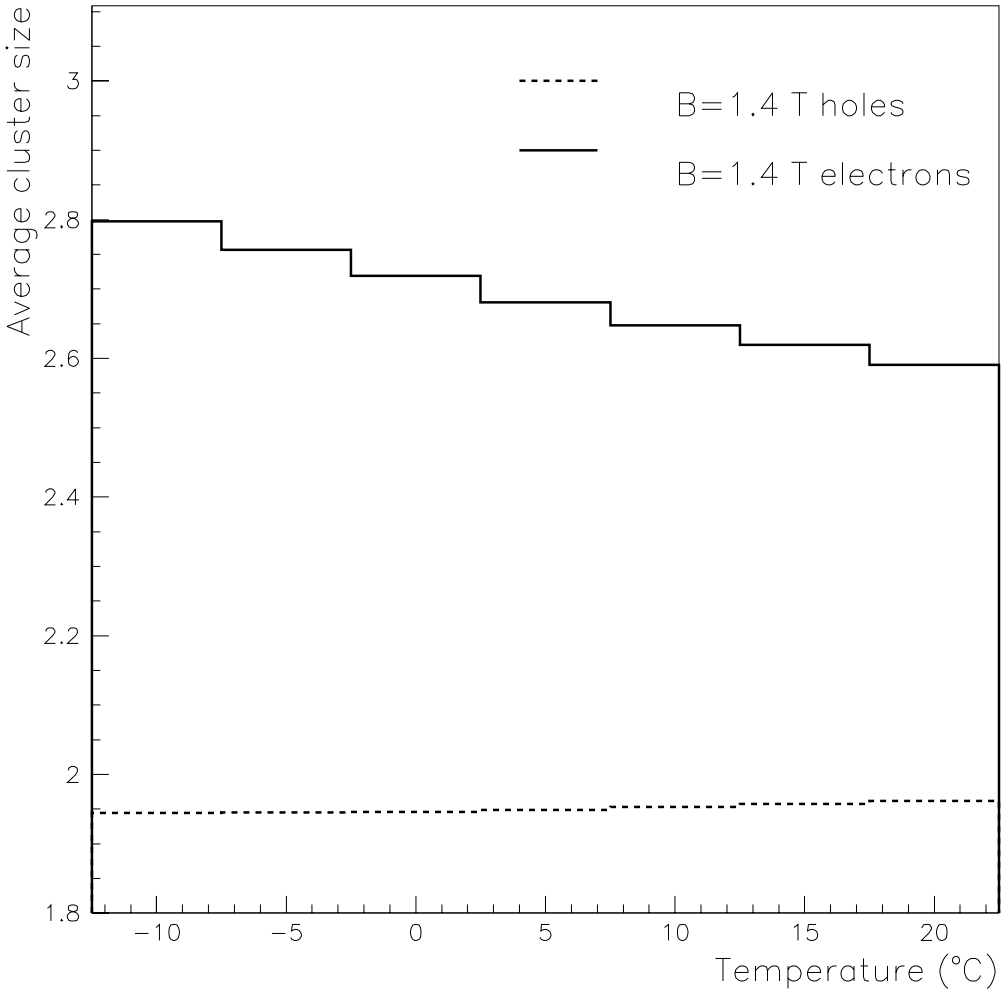

Figure 9: Average cluster size for normal incidence tracks as a function of temperature for a 60 μm sensor with small angle stereo strips on the n-side. As expected the shift due to the magnetic field gets smaller increasing the temperature (mobilities gets smaller increasing T). To enhance the effect the noise and the δ-rays have been turned off.

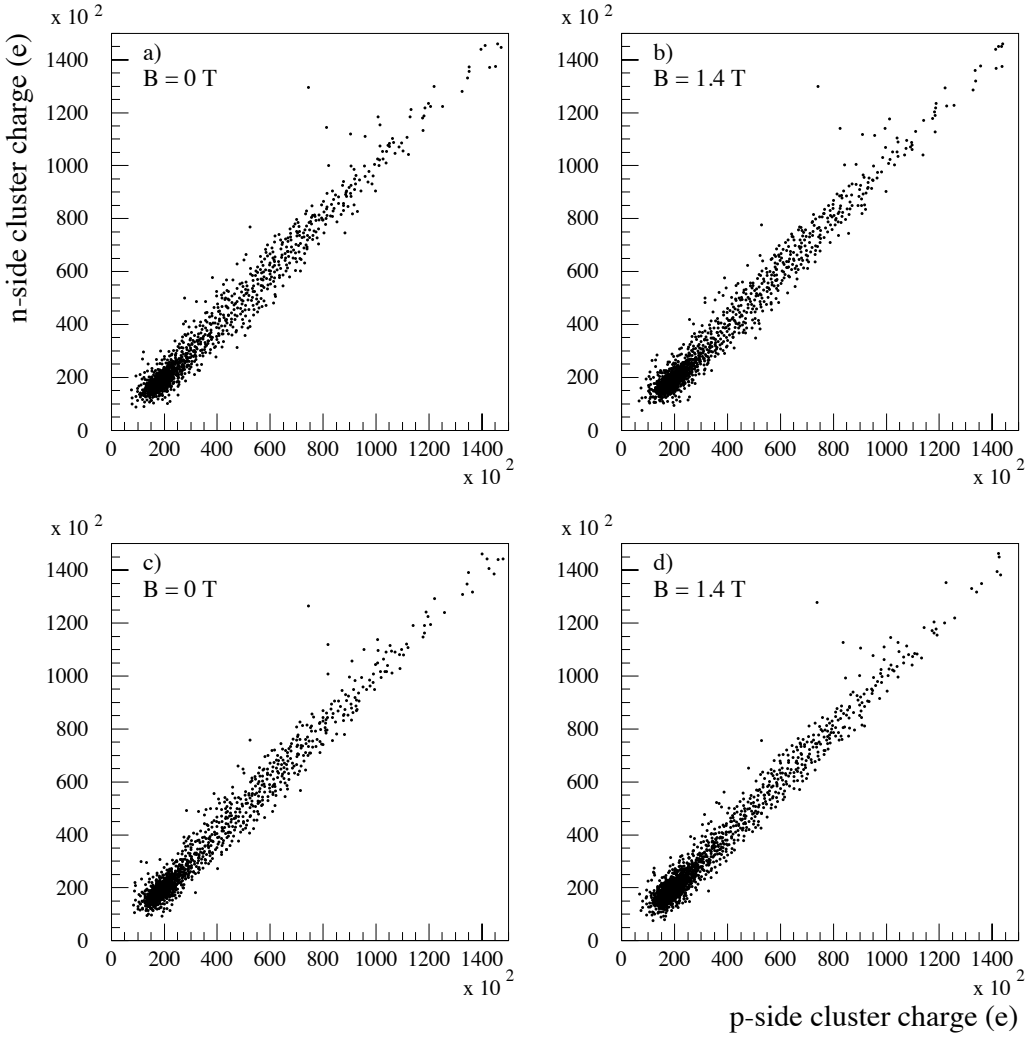

Figure 10: Charge correlation between clusters reconstructed on the p-side and n-side for SVXII type sensors with and without magnetic field: *a*) and *b*) $p(n)$-side= 60(140) μm pitch with 90^o stereo on the n-side; *c*) and *d*) $p(n)$- side= 60(60) μm pitch with small angle stereo on the n-side. Tracks are at normal incidence, noise is 1000 e

3 Comparison with data

In this section the model described above will be compared with actual data: in the first case from a Test Beam of a Run 2 type sensor and in the second with the old Run1 SVX' data. We want to stress that the knobs "tunable" for this model are very few once the specific characteristics of the sensor and running conditions have been specified.

3.1 Test Beam 1997

The data shown here come from the 1997 Test Beam performed at MT6 with a 150 GeV pion beam (m.i.p. with negligible multiple scattering). The setup comprised of a telescope (anchor planes) of four double sided Silicon sensors with 90^o stereo implant on the n-side. The two central slots were used for the sensors under test. All the setup was inside a Peltier box that kept the sensors at an effective temperature of 12^o C. We will compare our MC to the data coming from a Hamamatsu Layer 1 sensor with 90^o stereo, 62.25 μm pitch on the junction side and 141 μm pitch on the ohmic side. Only the junction side has been read out. The input parameters used in our simulation are shown in Tab.1. There are essentially only two tunable parameters: the amount of lost charge and the cross talk. The first one takes in account the shift on the peak of the Landau as in Fig.11. In Fig.12 we compare the contribution to the total charge from the distinct cluster sizes. The agreement is very good also for the cluster size distribution, see Fig.13, and from Fig.14 is visible the contribution of the δ-rays and the diffusion. Finally Fig.15 shown the residuals distribution obtained from the simulation, Δ = (*reconstructed position - true position*), the value of the rms of 13 μm reproduces what is measured on the data[6][5]. Clustering requires a seed strip with a charge greater than 5σ and then looks for a set of adjacent tracks over 4σ.

[6]The shape of the two and three strip cluster residuals is purely due to the fact that the clustering algorithm assumes a flat distribution of charge instead of the correct gaussian shape. This geometrical effect is easier to see in these context (wrt to Run1 data) due to the high signal to noise and the perpendicular incidence of the tracks.

Input Test Beam 1997	
p	150 GeV
θ	90^o
B	0. T
pitch(p-side)	0.00622 cm
T	12^oC
V_{dep}	40 V
V_{bias}	70 V
Noise	590 e
x-talk	8.35 %
F_{lost}	25 %

Table 1: Summary of the input parameters used in the simulation to make the comparison with the 1997 Test Beam data (SVXII L1 Hamamatsu sensor)

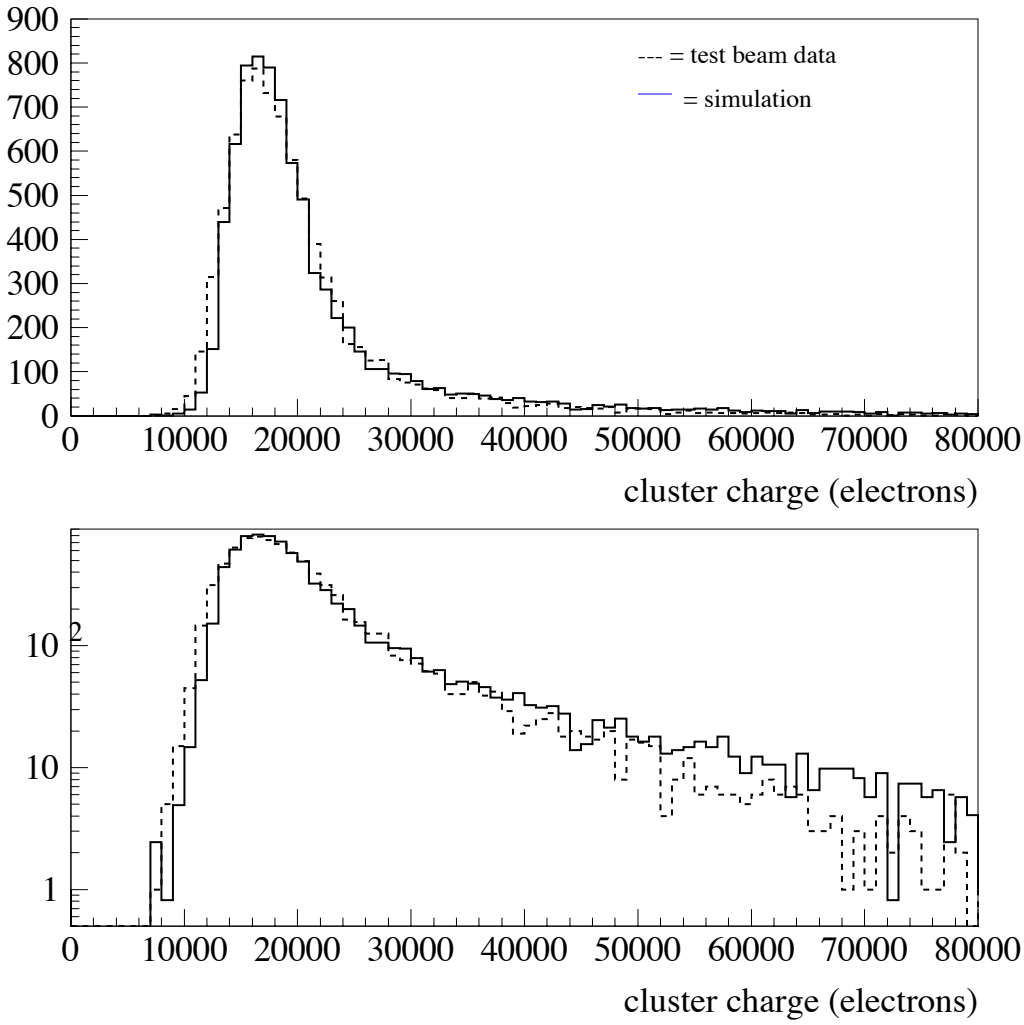

Figure 11: Cluster charge of p-side for Hamamatsu sensor DB12 used in 1997 Test Beam compared with the simulation. All cluster sizes considered. Top plot: linear scale; Bottom plot: log scale.

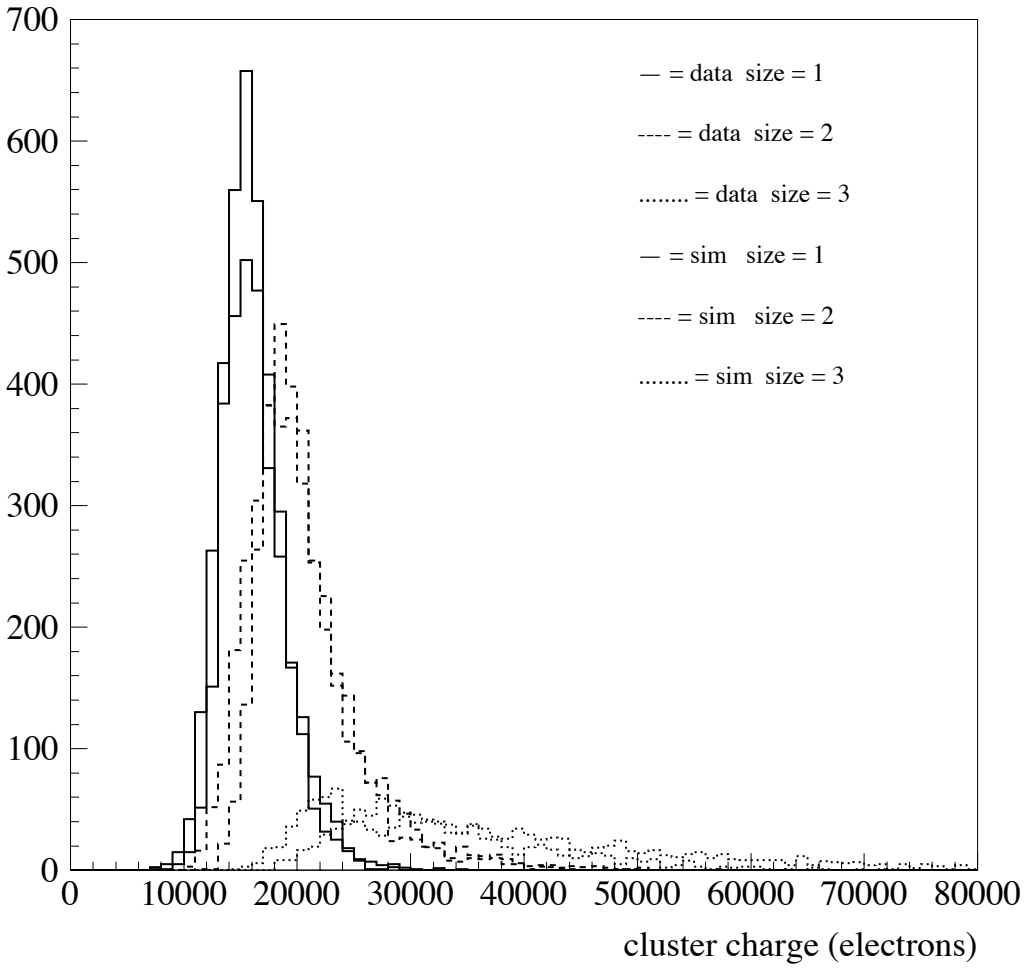

Figure 12: Cluster charge of p-side for Hamamatsu sensor DB12 used in 1997 Test Beam compared with the simulation. The distribution of the charge for clusters with $n = 1, 2, 3$ strips are compared separately with the simulation.

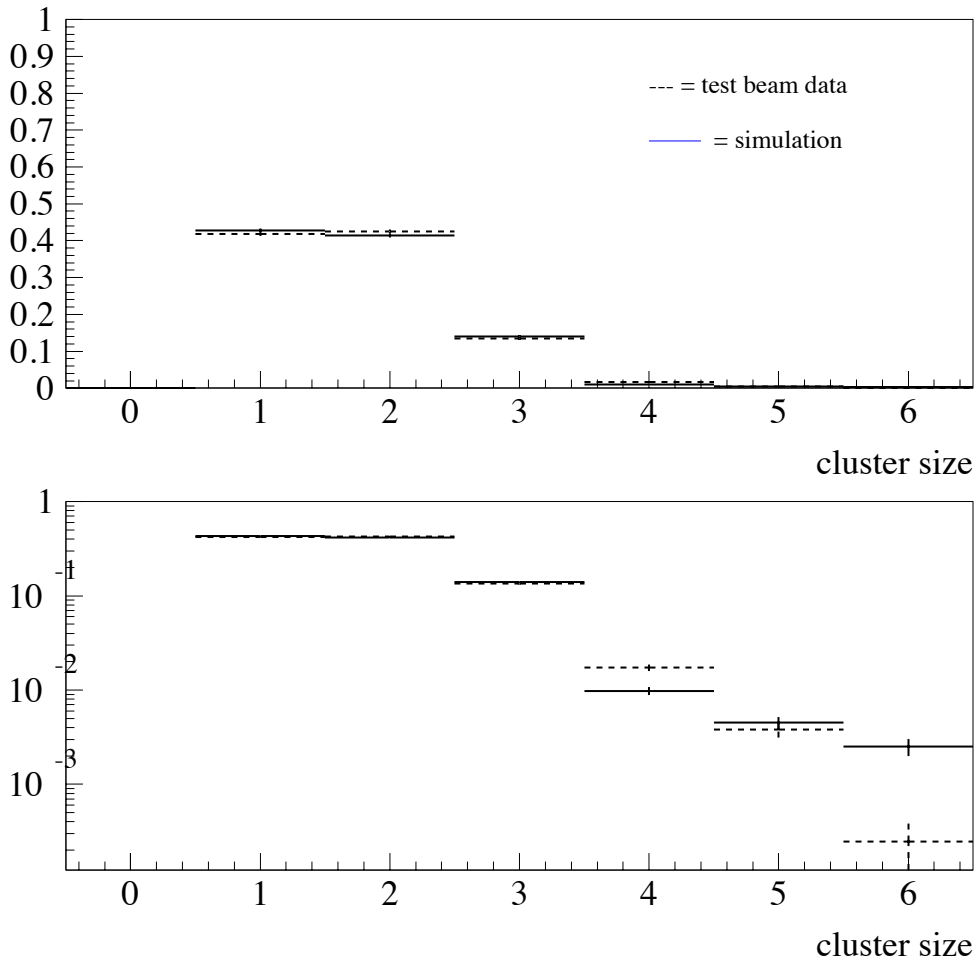

Figure 13: Cluster size of p-side for Hamamatsu sensor DB12 used in 1997 Test Beam compared with the simulation. Top plot: linear scale; Bottom plot: log scale.

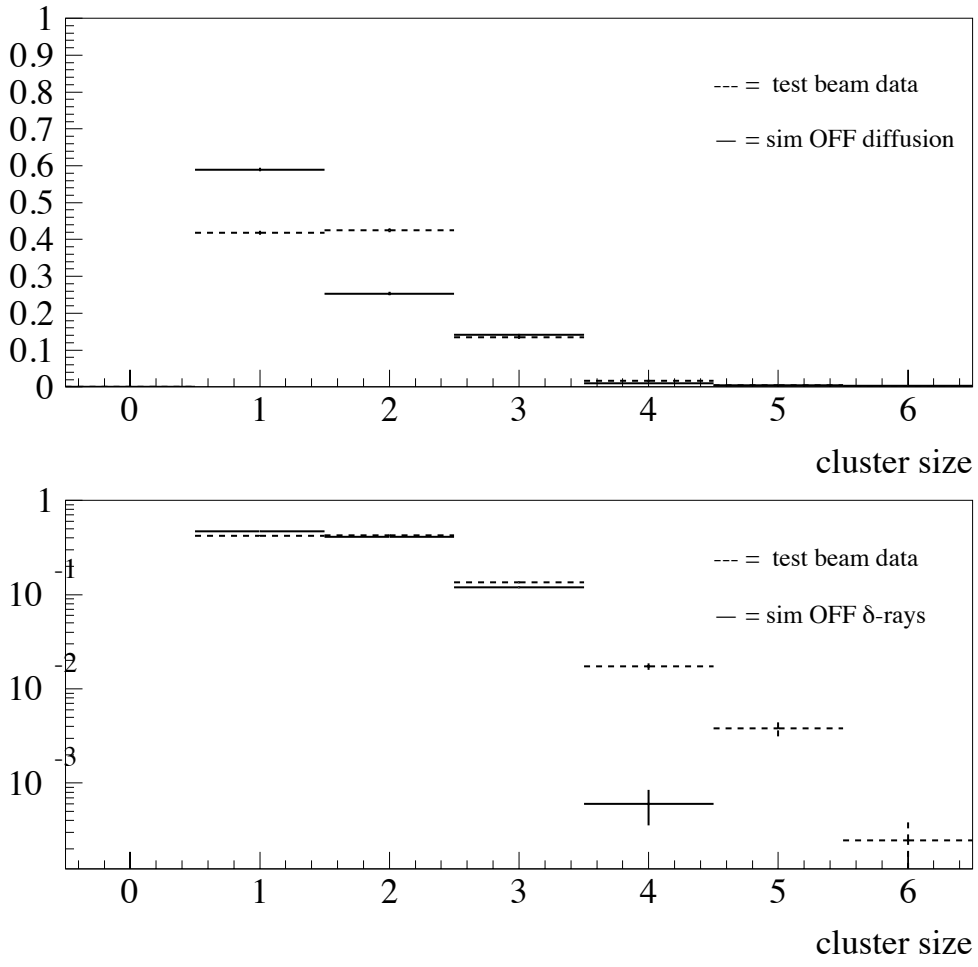

Figure 14: Cluster size of p-side for Hamamatsu sensor DB12 used in 1997 Test Beam compared with the simulation with some of the effects turned off: diffusion off (top plot, linear scale), δ-rays off (bottom plot, log scale).

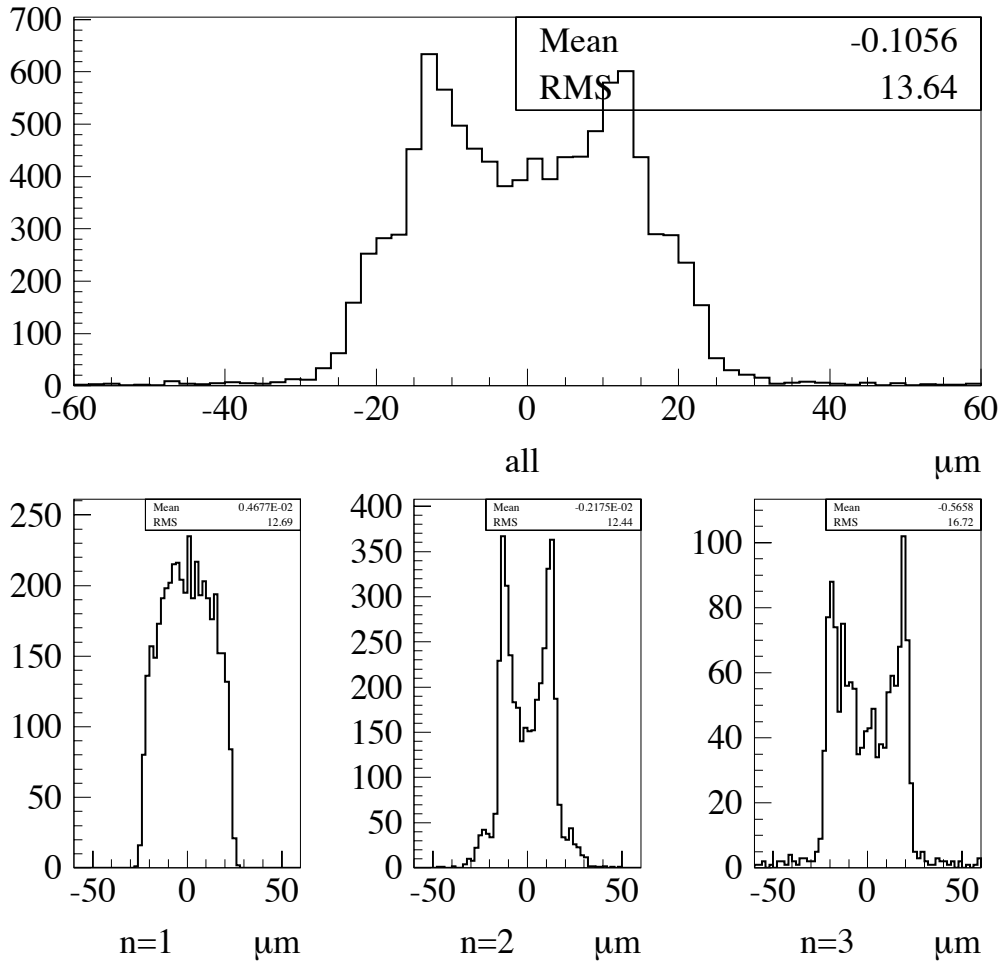

Figure 15: Residuals distribution obtained from the simulation of the Hamamatsu sensor DB12 used in 1997 Test Beam: all cluster sizes (top plot) and distribution for the separate cluster sizes (bottom plot). The RMS value is consistent with the measurement of 13 μm obtained on the data.

3.2 Run 1 SVX' data

A very significant test is to compare our simulation with the Run1 SVX' data. The set of data used[7] is the same one that served to develop the SVX' MC simulation: for a description of the sample see [6]. The parameters of the simulation (x-talk and F_{lost}) have been tuned using the data only in the angular regions $\Delta\Phi = \pm 4^o$ and $\Delta\Theta = \pm 30^o$. F_{lost} is chosen so that we reproduce the shift in the Landau peak at 19,000 e for $S/N \simeq 13$. The value of x-talk at 2% is somewhat lower than expected (5%).

In Fig.16 and Fig.17 the total cluster charge and the cluster size distribution are shown: it should be noticed the good description of the large size cluster due to the presence of δ-rays.

The residuals distribution for separate cluster sizes are shown in Fig.18; the values are somewhat smaller but consistent with the measured ones:

- n=1, $\sigma_{measured} = 13 \pm 1\mu$m while $\sigma_{sim} = 12\mu$m
- n=2, $\sigma_{measured} = 11 \pm 1\mu$m while $\sigma_{sim} = 8\mu$m
- n=3, $\sigma_{measured} = 19 \pm 1\mu$m while $\sigma_{sim} = 17\mu$m

The shift due to the magnetic field is of about 10 μm consistent with the expectations.

In Fig.19 and Fig.20 the distributions of cluster size and total cluster charge are shown for several angular regions in Φ and θ.

There is a reasonable agreement everywhere, even if the toy MC used considers a track in a single layer of Silicon instead of having the full detector geometry with all the effects of misalignments, different track p_T, detector noises and bias voltages etc.

[7]Thanks to J. Incandela and D. Stuart.

Input Run1 SVX' data	
p	5 GeV
θ	$\in [0^o, 45^o]$
ϕ	$\in [0^o, 12^o]$
B	1.41 T
pitch(p-side)	0.0060 cm
T	$20\,^o$C
V_{dep}	30 V
V_{bias}	45 V
Noise	1400-1500 e
x-talk	2.0 %
F_{lost}	26 %

Table 2: Summary of the input parameters used in the simulation to make the comparison with the Run 1 SVX' data

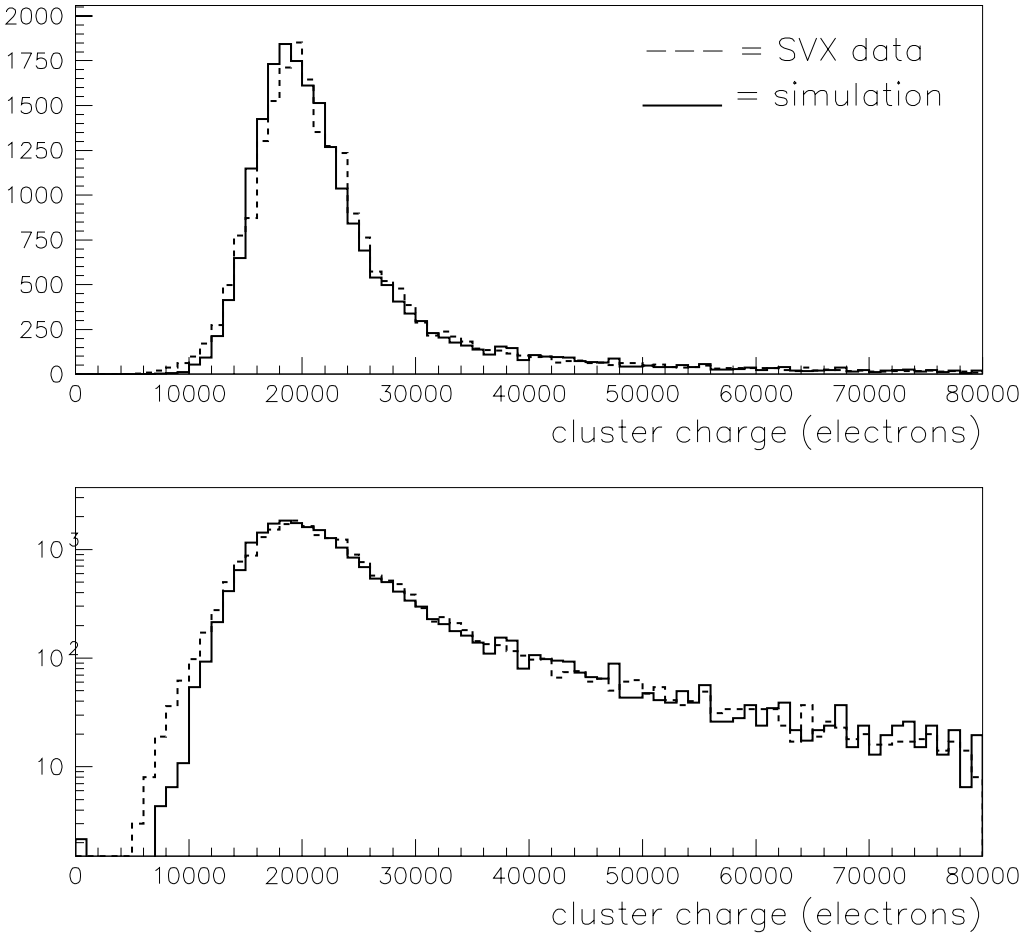

Figure 16: Cluster charge distribution for tracks in the range $\Delta\Phi < 12^o$ and $\Delta\theta < 30^o$: SVX' data (dash) are compared with the simulation (line). Top plot: linear scale; Bottom plot: log scale.

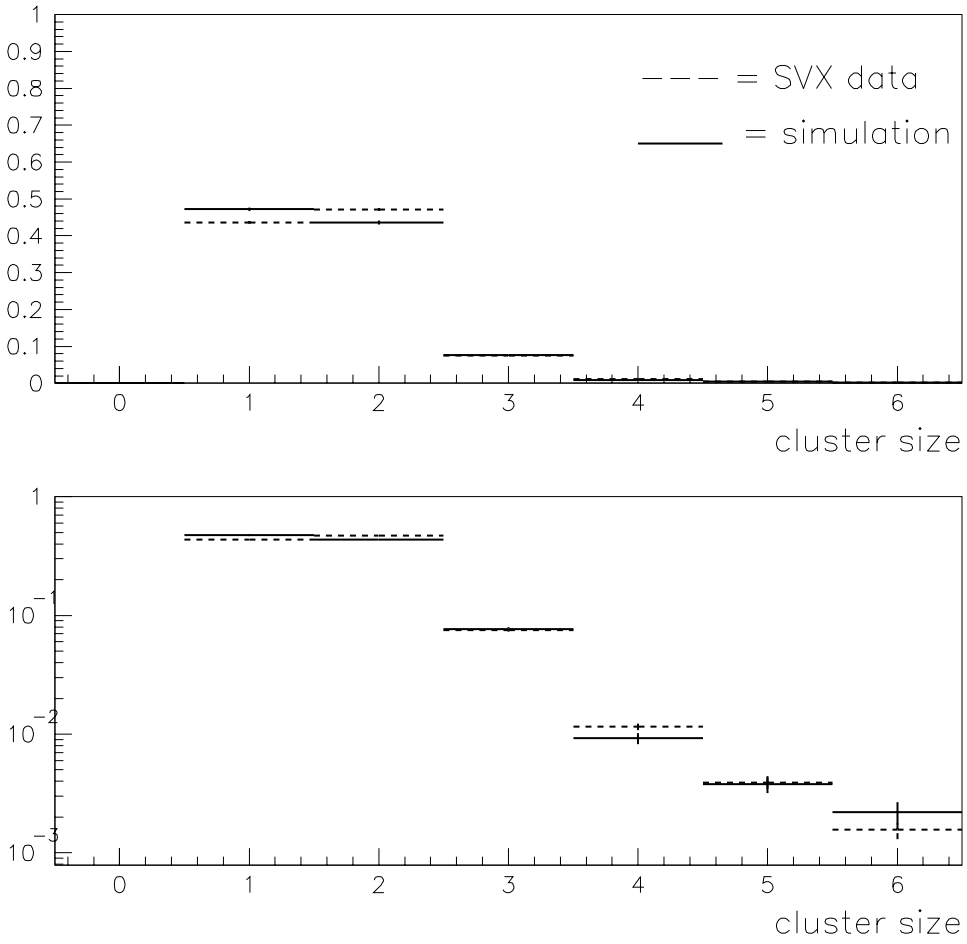

Figure 17: Cluster size distribution for tracks in the range $\Delta\Phi < 12^o$ and $\Delta\theta < 30^o$: SVX' data (dash) are compared with the simulation (line). Top plot: linear scale; Bottom plot: log scale.

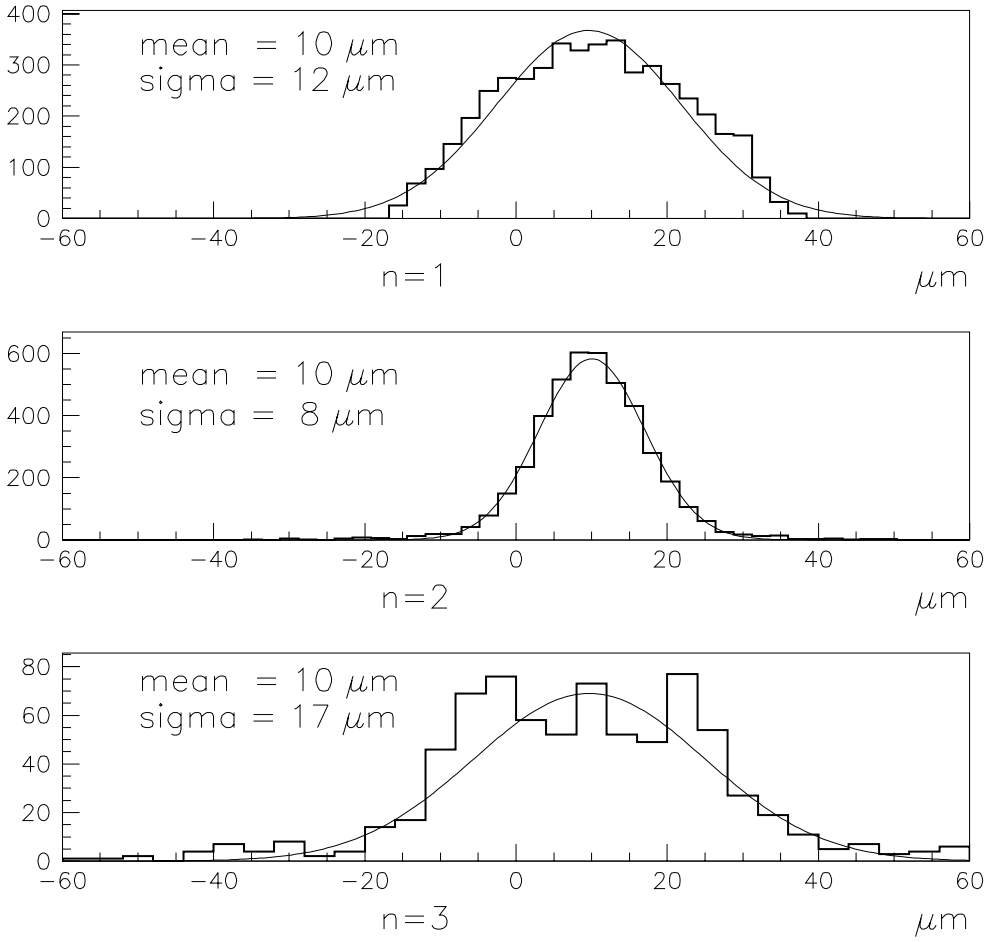

Figure 18: Residuals distribution for simulated tracks in the range $\Delta\Phi < 12^o$ and $\Delta\theta < 30^o$. See text for the consistency of the numbers with the actual Run1 SVX' measurement.

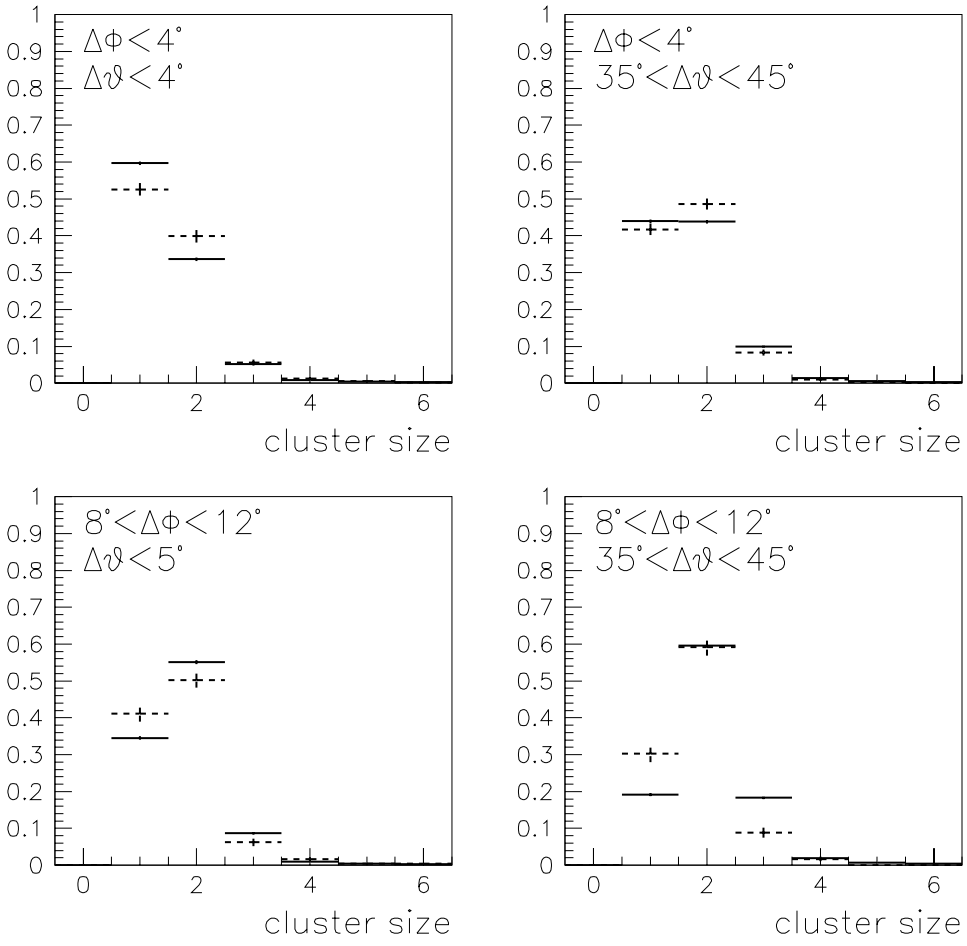

Figure 19: Cluster size distribution for tracks in various angular ranges for SVX' data (dash) compared with the simulation (line). Note that the simulation has been tuned using tracks in the range $\Delta\Phi < 12^o$ and $\Delta\theta < 30^o$.

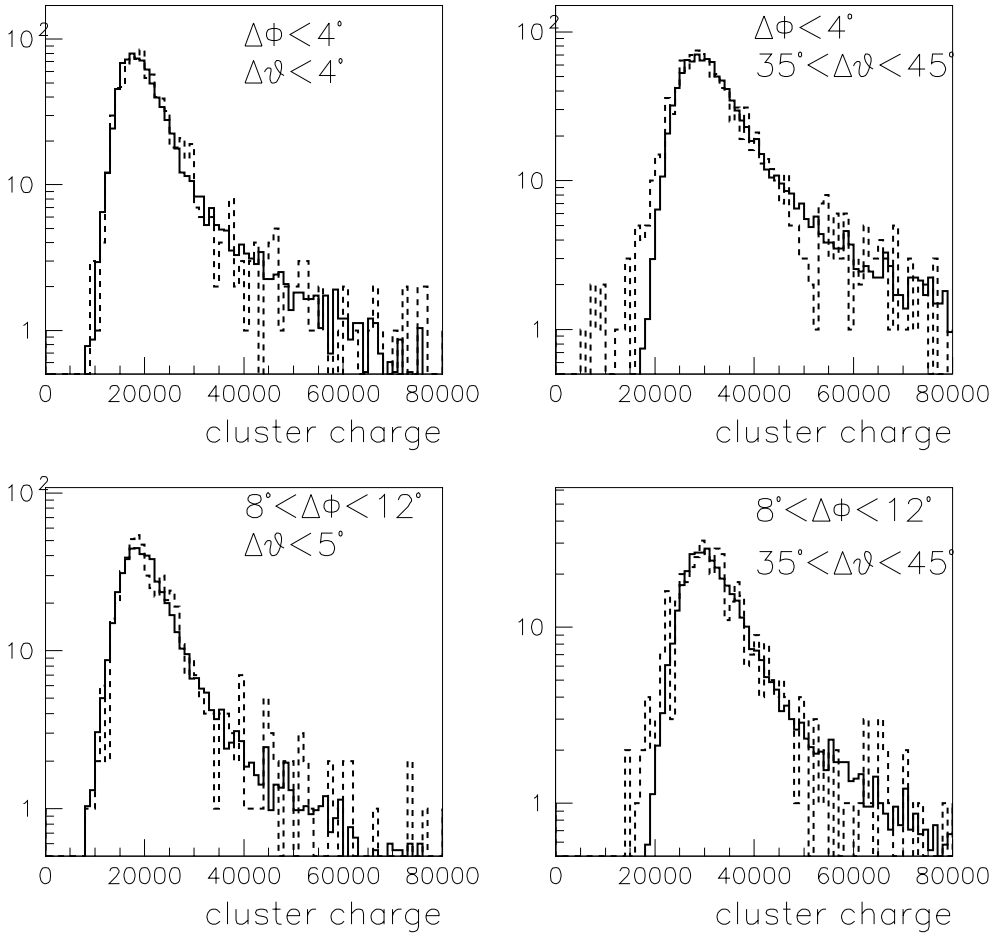

Figure 20: Cluster charge distribution for tracks in various angular ranges for SVX' data (dash) compared with the simulation (line). Note that the simulation has been tuned using tracks in the range $\Delta\Phi < 12^o$ and $\Delta\theta < 30^o$.

4 Studies for L00 project

This stand-alone toy MC has the flexibility that allows to study the performances of possible configuration for future detectors. In particular we report here the summary of a study done for the L00 project[7]. The goal is to compare the performances in terms of single track resolution and two track separation of three different configuration: 50 μm physical and readout pitch, 50 μm readout pitch with an intermediate floating strip (effective pitch 25 μm) and 25 μm physical and readout pitch. The study has been done for different region of signal to noise ratio (S/N=10 being the closest to the final configuration). This study required to implement the floating strip configuration in the MC simulation. The generation of the signal is then modified as follows: the charge is generated from a Landau distribution and corrected for the fraction lost. δ-rays and the ionization charge is then diffused toward all the physical strips. Then the charge collected by the floating strip is reduced by a 25% inefficiency (typical value) and the remainder is divided between the two adjacent strips connected to the readout. Finally the cross talk between the readout strips is considered and the noise added. The summary of the parameters used is in Tab.3.

Input L00 study	
p	5 GeV
θ	normal incidence
ϕ	normal incidence
B	1.41 T
pitch(p-side)	0.0025 and 0.0050 cm
T	5 °C
V_{dep}	80 V
V_{bias}	100 V
Noise	see text
x-talk	4.0 %
F_{lost}	20 %
Floating strip inefficiency	25%

Table 3: Summary of the input parameters used in the simulation to make the study for L00

Two different clustering algorithms have been used. One can be considered a "perfect" clustering for normal incidence tracks, because it considers the strip that is actually hit plus the two closest neighbours (if they are above $2\sigma_{noise}$). The cluster position is obtained as the total charge centroid. The second, called "SVT clustering", defines a cluster as a contiguos set of strips above a single threshold value (indipendent from the cluster length). The maximum cluster length is 6 strips. The cluster position is obtained as the charge centroid for length less than four strips and as the geometric median for clusters size four or bigger.

4.1 Single hit resolution

The main effect of the addition of an intermediate floating strip is to increase, for the case of normal incidence particles, the number of two strip clusters with respect to the single strip ones. Infact this corresponds (for a sufficient S/N) to an improvement in the hit resolution. See in Fig.21 the cluster length distribution for normal incidence tracks in the three cases considered. First of all we are interested in the behaviour of the position resolution for a normal incidence track as a function of the signal to noise and of the strip charge threshold for the three different configurations: see Fig.22 and Fig.23. As expected in the S/N$\simeq$ 10 region having a floating strip improves the resolution for the 50 μm readout of about 20%. In case of very high S/N the floating strip allows to almost fully recover the resolution achievable with a 25 μm readout pitch. In Fig.24 are plotted the resolutions obtained from the "perfect clustering" as a function of the S/N for the three cases that have then to be considered as upper limits.

4.2 Two hit separation

For the study of the two hit separation the toy montecarlo has been modified to have two tracks generated at the same time varying the distance between them. In the case of the "SVT clustering" we count the number and the position of the separate cluster found. For a "perfect" approach we consider instead all the strip above a small threshold and define the presence of two tracks and their position if there are to distinct maxima with a dip in the middle. In Fig.25 is plotted, for the 50 μm with floating strip, the shape of the charge distribution on 10 strips around the tracks as the distance between the tracks is varied. In Fig.26 it is shown for the three configuration the fraction of resolved two tracks events as a function of the distance of the hitting tracks using the "perfect" approach of finding the relative maxima. For the case of 50 μm with floating strip we resolve 90% of the events when they are 90 μm apart. However when we employ a more realistic clustering, like the "SVT", the minimum separation needed to resolve 90% of the cases is about 130 μm, as is shown in Fig.27. In Fig.28 the residual distribution for this clustering algorithm is shown.

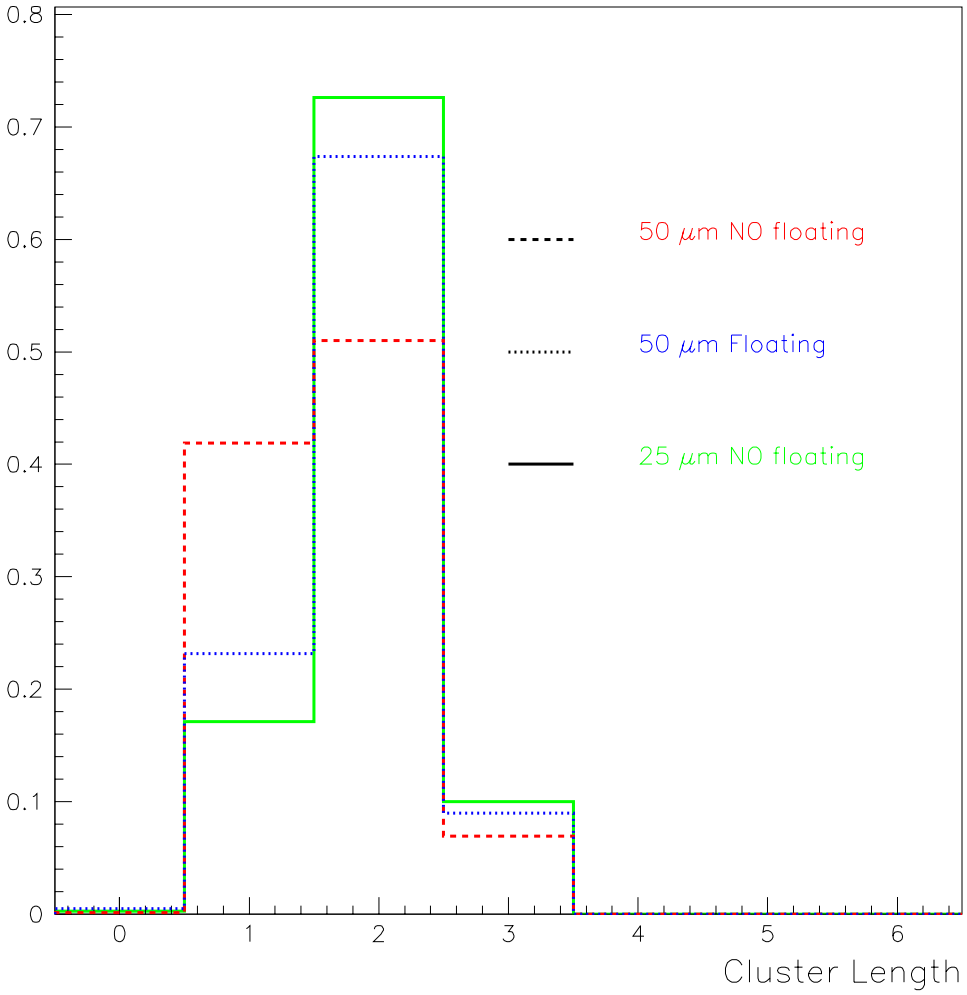

Figure 21: Distribution of the cluster length for the three configurations studied for the L00 sensor. The presence of an intermediate floating strip provides an increase in the number of two strip cluster for normal incidence tracks.

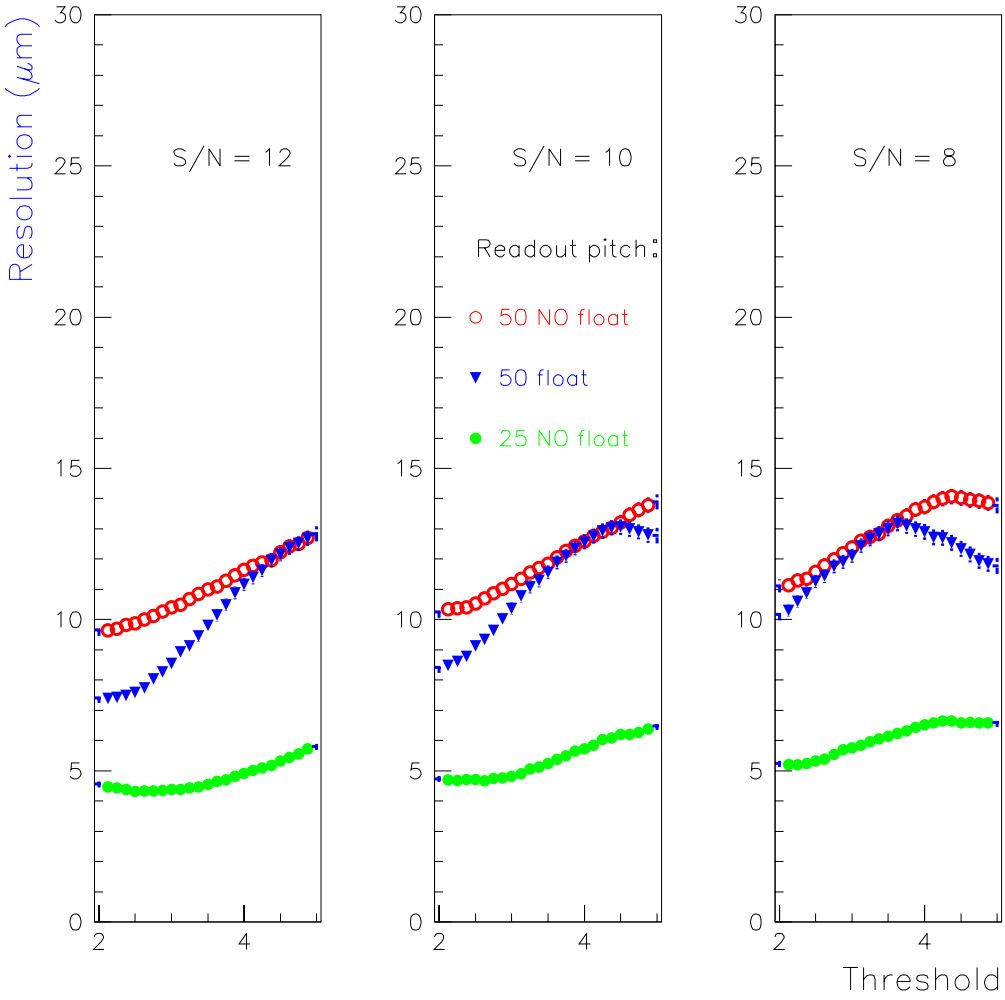

Figure 22: Single hit position resolution for different S/N situations as a function of the σ noise threshold for the "SVT clustering". Default cut is at 2σ noise. The improvement due to the presence of an intermediate floating strip is strongly dependent on the S/N ratio, for S/N=10 the improvement is of about 20%.

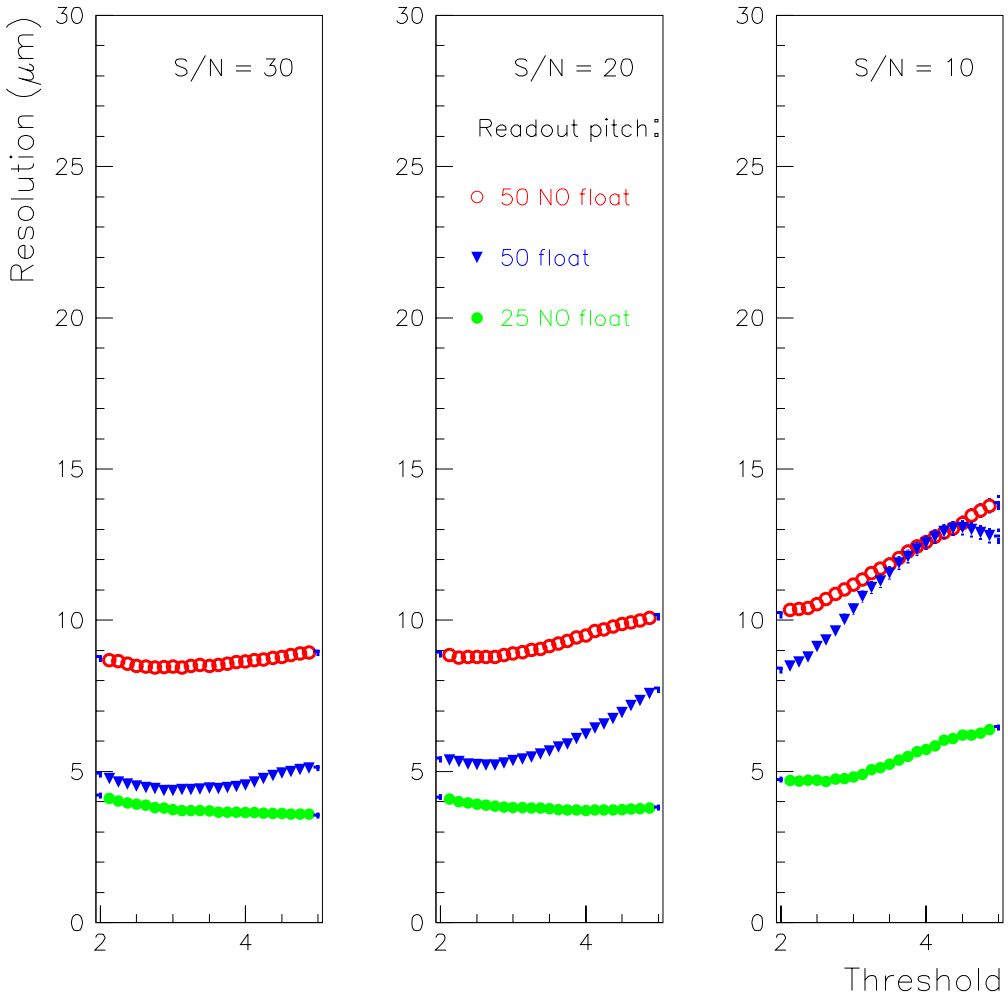

Figure 23: Single hit position resolution for different S/N situations as a function of the σ noise threshold for the "SVT clustering". Default cut is at 2σ noise. For very large values of S/N the presence of the floating strip with a 50 μm readout pitch almost fully recovers the resolution achievable with a 25 μm readout pitch.

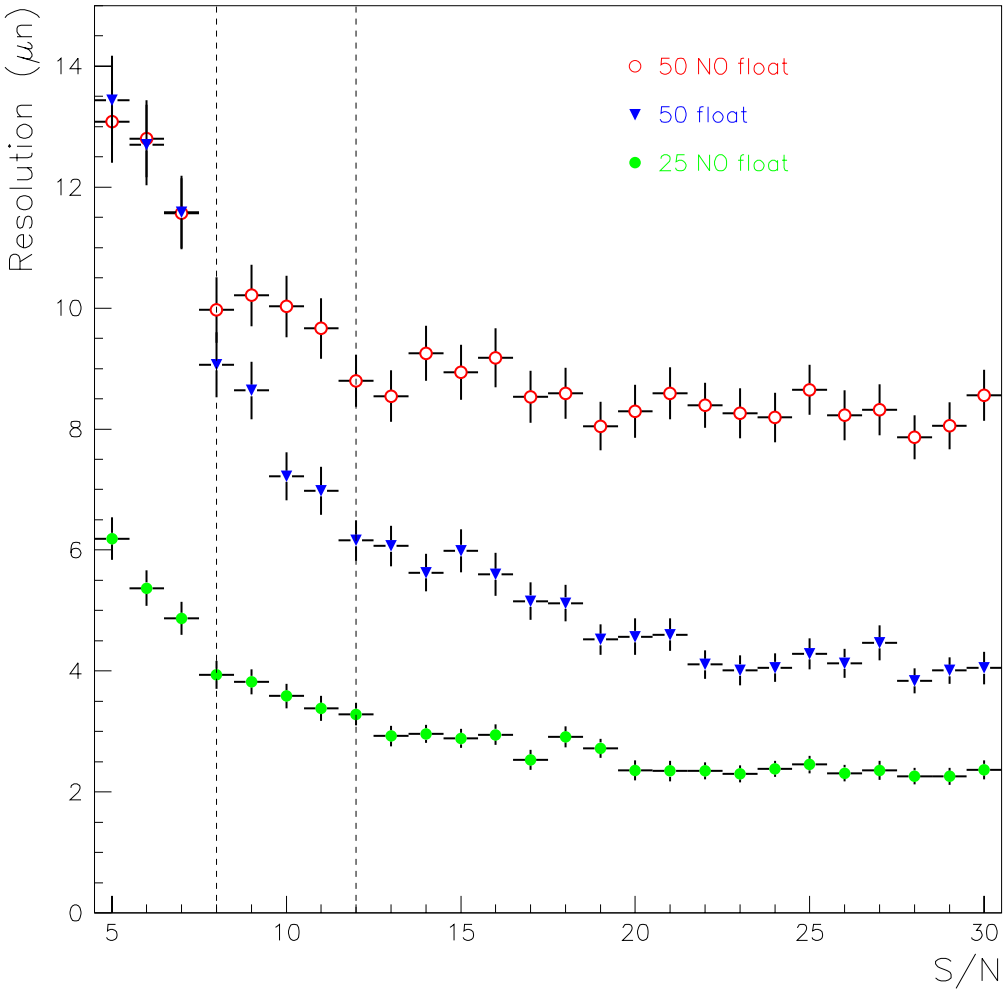

Figure 24: Single hit position resolution as a function of the S/N ratio for the three different configuration. The values obtained here are to be considered as upper limits ("perfect clustering" algorithm used).

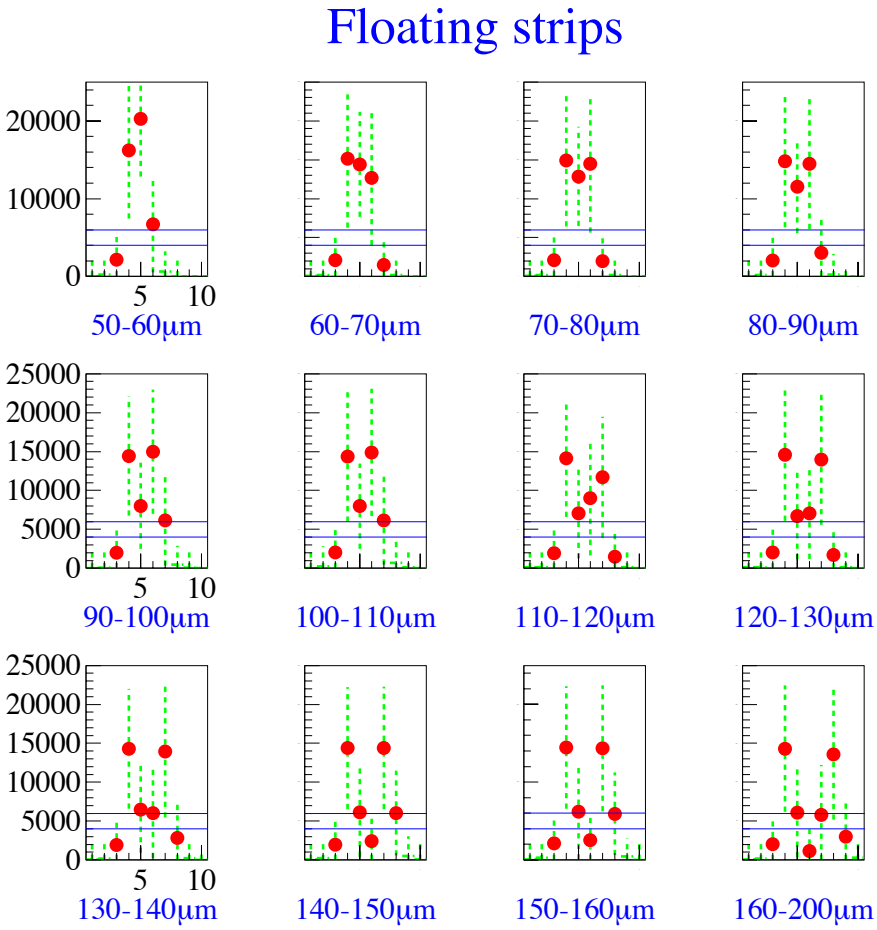

Figure 25: Distribution of the average charge in the strips for different distances between the two hitting tracks for the configuration of a 50 μm readout with an intermediate floating strip.

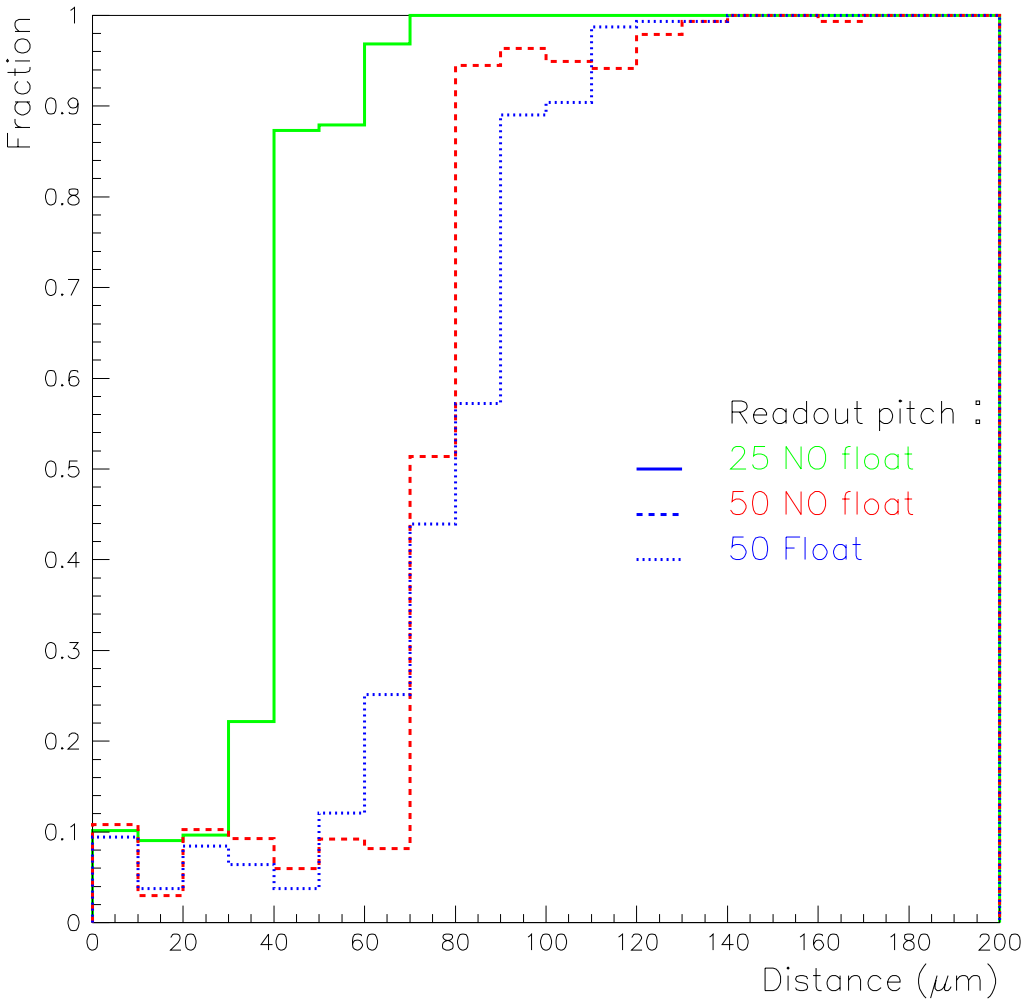

Figure 26: Fraction of fully resolved two hit events as a function of the distance between the two hitting tracks. For the case of 50 μm with floating strip, the fraction of resolved two hits is about 90% when the hits are at least 90 μm apart. This is an upper limit because we have employed a "perfect" hit finding approach based on the presence of relative maxima.

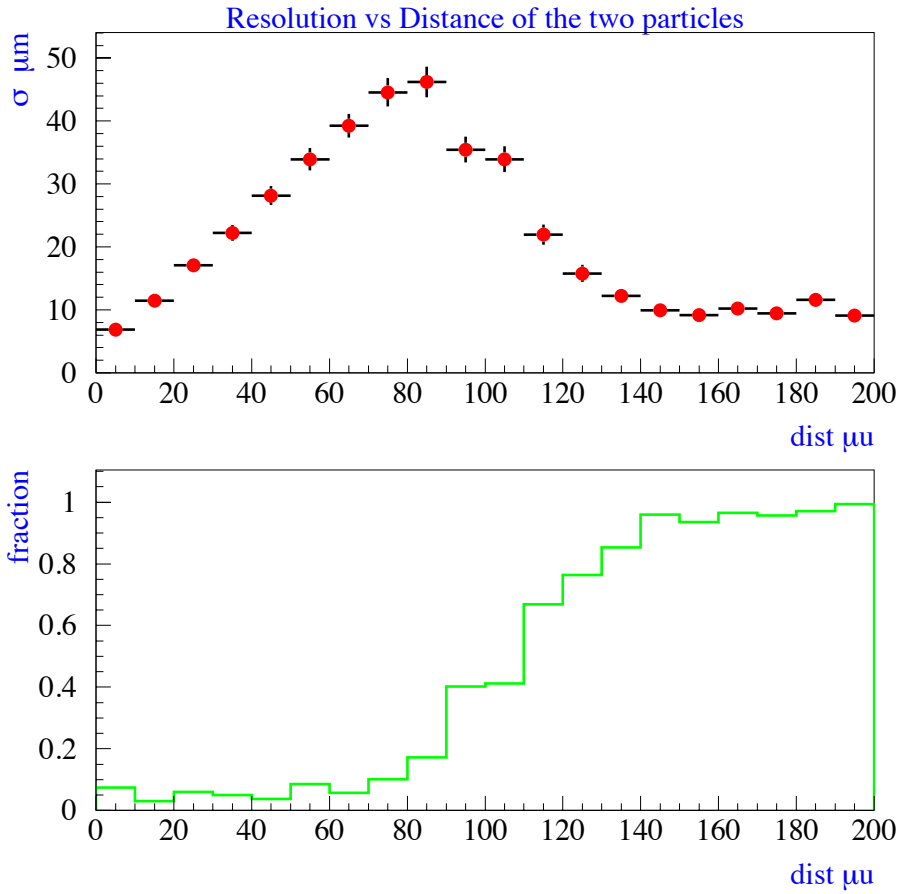

Figure 27: Hit resolution (top) and fraction of resolved two hit events (bottom) as a function of the distance between the two hitting tracks for the case of 50 μm readout pitch with floating strip. The more realistic "SVT clustering" has been used here. The minimum distance needed to resolve 90% of the events is about 130 μm.

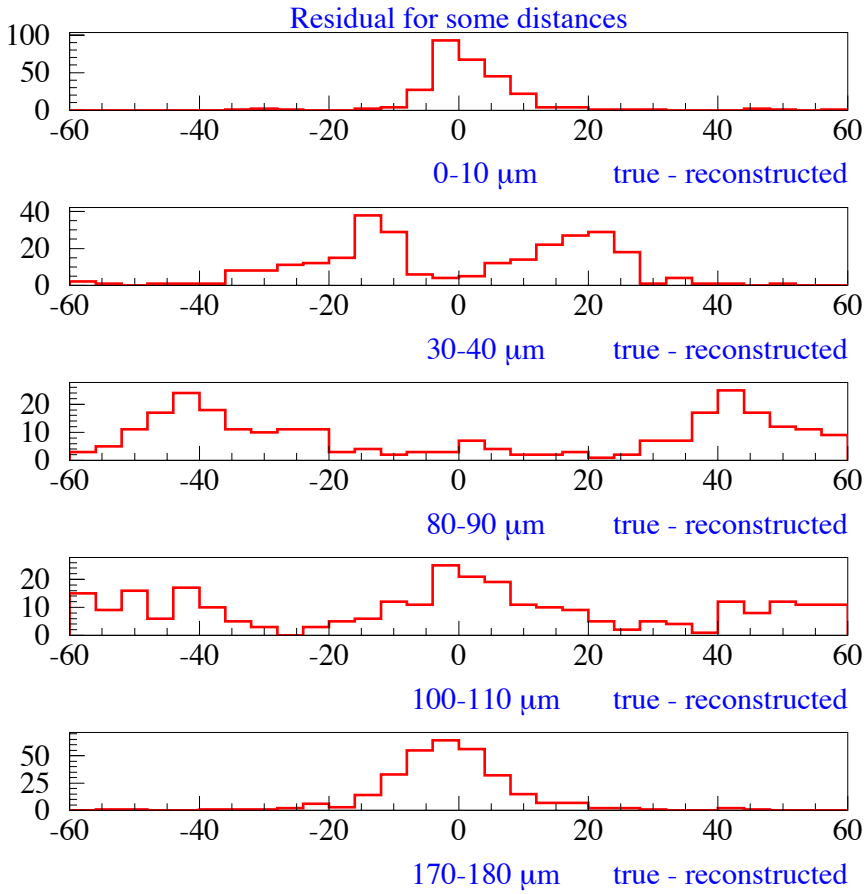

Figure 28: Residuals distribution for two tracks events for the case of 50 μm readout pitch with floating strip. "SVT clustering" used. Residual is defined for each track as Δ = *reconstructed position - true position* (always two entries per event). If two clusters are found, the closest to the track is used.

5 Conclusion

In this note has been described a model for charge deposition in Silicon detectors that is based only on first principles. The model includes diffusion and δ-rays treatment and the effect of magnetic field. Noise and readout effect are also included. The comparison with Test Beam data from a SVXII-type sensor and Run1 SVX' data shows a very good agreement between data and this MC. This model is implemented in a stand–alone code that resides in the Run2 CVS repository in a package called `toySiChargeDep`. In the same area there are instruction on how to run the code and obtained plots of the significant quantities (filename `README`). This model is also implemented in the official Run2 silicon simulation and can be turned on via a talk-to.

6 Acknowledgements

We'd like to thank Joe Incandela and David Stuart for their help and suggestions. Also, we thank Matthew Herndon for the inclusion of this model within the official RunII simulation package.

References

[1] PDG 23.2.5 pg.146

[2] G. Hall, "Ionization Energy Losses of Highly Relativistic Charged Particles in Thin Silicon Layers", NIM 220 (1984) 356-362

[3] PDG 23.2.6 pg.146

[4] Tabata,Ito and Okabe, NIM 103 (1972) 85

[5] R. Rossin, Tesi di Laurea, Universita' di Padova, 1998

[6] "The SVX' MC Simulation", CDF Note 2946 (1995)

[7] "Layer00 Proposal", CDF Note 4924 (1999)